
Article:
Wang, L., Chen, L., Provis, J.L. orcid.org/0000-0003-3372-8922 et al. (2 more authors) (2020) Accelerated carbonation of reactive MgO and Portland cement blends under flowing CO2 gas. Cement and Concrete Composites, 106. 103489. ISSN 0958-9465

https://doi.org/10.1016/j.cemconcomp.2019.103489

Accelerated Carbonation of Reactive MgO and Portland Cement Blends Under Flowing CO_2 Gas

Lei Wang[1,2], Liang Chen[1], John L. Provis[2], Daniel C.W. Tsang[1,*], Chi Sun Poon[1]

[1] Department of Civil and Environmental Engineering, The Hong Kong Polytechnic University, Hung Hom, Kowloon, Hong Kong, China.

[2] Department of Materials Science and Engineering, The University of Sheffield, Sir Robert Hadfield Building, Mappin St, Sheffield S1 3JD, United Kingdom.

[*] Corresponding author: dan.tsang@polyu.edu.hk

Abstract

The use of MgO-based materials for sequestration of CO_2 offers technical advantages and environmental incentives. However, the understanding of accelerated carbonation of MgO-based materials in flowing CO_2 gas is limited. This study elucidates the carbonation behaviour of reactive MgO cement (MC) and MgO-Portland binary cement (BC) in a simulated CO_2-rich industrial exhaust. Quantitative X-ray diffraction and thermogravimetric analyses showed that nesquehonite ($MgCO_3 \cdot 3H_2O$) was the major carbonation product in MC pastes, whereas $CaCO_3$ was preferentially generated in BC pastes. The relative humidity of exhaust gas influenced CO_2 diffusion and the carbonation rate; 98% humidity facilitated MC carbonation whereas 50% was favourable for BC carbonation. Although CO_2 concentration determined the carbonation rate, 10% CO_2 gas in the exhaust was sufficient to accelerate carbonation. The carbonation degree and compressive strength of samples cured for 7 days at 10% CO_2 were comparable to the values of samples cured for 1 day at 100% CO_2. The presence of acid gases during CO_2 curing inhibited the carbonation and hydration processes, but the presence of Portland cement in the BC system gave good compatibility with acids and relieved the inhibitory effect. Desulphurization and denitrification of industrial exhaust gas are nonetheless

desirable before CO_2 curing. This study builds the foundation for utilising industrial CO_2 exhaust to accelerate the carbonation of Mg-based materials.

Keywords: eco-friendly cement; CO_2 sequestration/utilisation; amorphous hydrated carbonate; cement hydration chemistry; gaseous waste valorisation; sustainable chemistry/engineering.

Graphical Abstract

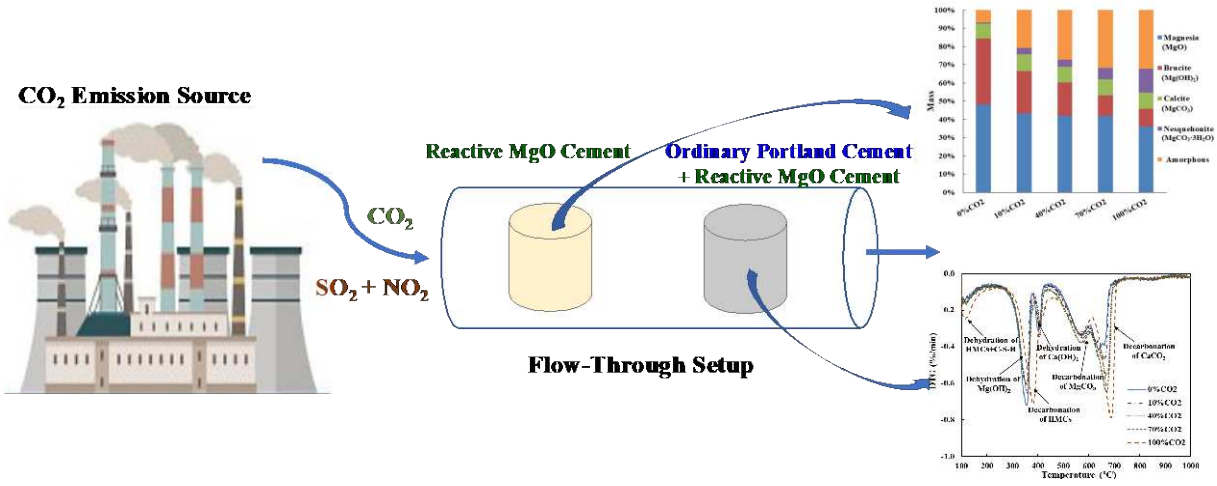

Highlights:

- MgO-based cement can sequester and utilize CO_2 from industrial exhaust.
- Relative humidity influenced CO_2 diffusion and carbonation rate.
- 7-d curing with 10% CO_2 concentration ensured sufficient carbonation degree.
- Acid gases in exhaust severely inhibited carbonation and hydration.
- Binary MgO-Portland cement showed fast carbonation rate and good compatibility with acids.

1. Introduction

Cement and concrete have been essential materials for the urbanisation of society. More than 10 billion tonnes of concrete are annually generated worldwide, which has been the second-most-used material in the world only behind water [1]. Concrete is usually based on ordinary

Portland cement (PC) as a binding material, due to its robust, reliable, and inexpensive nature. PC is generated from calcination of limestone and clay minerals at 1400 °C in a kiln, which is associated with a high CO_2 emission (660–820 kg CO_2 per tonne) contributing to approximately 7-10% of global anthropogenic CO_2 emissions [2-4]. Therefore, extensive research has been devoted to developing alternative low-carbon cementitious systems to partially or totally replace PC in certain applications.

Reactive magnesia cement (MC) is a promising candidate "green cement", produced by the calcination of magnesite at relatively low temperature (650–800 °C) [5,6]. Recently, recovery of Mg^{2+} from salt lakes and seawater to produce MC has been proposed as an eco-friendly approach [7], as the low geological abundance of high-purity magnesium minerals in many parts of the world constrains the uptake of magnesia-based cements [8]. However, in locations where suitable resources are available at scale, this is a potentially attractive route to valorisation of under-utilised resources. For instance, as a by-product of the Li_2CO_3 production from salt lakes, there are 200,000 tonnes of MgO produced annually in Qarhan Salt Lake in Qinghai Province, China [9]. Partial MC replacement in PC-based cementitious binder systems could enhance the properties of cement and concrete products, including characteristics such as denser pore structure, higher mechanical strength, superior resistance to chemical attack and corrosion, as well as excellent compatibility with contaminants [10,11].

Recent research has shown that MC is a versatile material that can be used alone as a binder, or blended with other materials for diverse applications, such as MgO expansive cements, MgO-based self-healing materials, MgO-based stabilization/solidification agents, MgO-modified alkali-activated materials, magnesium phosphate cements, magnesium oxychloride (Sorel) cements, magnesium oxysulphate cements, magnesium silicate hydrate (M-S-H)

cements, and others [8,12,13]. Importantly, MC derived from an efficiently-produced magnesia source is regarded by some as a "carbon negative" cementitious material, as it can sequester CO_2 and gain improved binding properties during accelerated carbonation [14,15]. CO_2 curing has been suggested to accelerate the carbonation of cement-based products and facilitate carbon sequestration in solid mineral phases [16,17]. During CO_2 curing, dissolved and ionised CO_2 induces the carbonation of Ca^{2+}/Mg^{2+} ions from the cement matrix, which then precipitates in the voids of the matrix as carbonates (anhydrous and hydrated) in a short period of time, boosting setting and hardening process, forming a dense, strong and potentially stable structure [18-20]. MC usually contains more than 85% active MgO, and the CO_2 sequestration capacity can reach up to 92.8 wt%, which is higher than the capacity of PC (50.4 wt%) based on theoretical calculation. The carbonation of MC can take place via the formation of magnesium carbonate ($MgCO_3$) from hydrated $Mg(OH)_2$ by the uptake of CO_2:

$$Mg(OH)_2 + CO_2 \rightarrow MgCO_3 + H_2O \quad \text{(Eq. 1)}$$

or with the incorporation of water to form hydrated magnesium carbonates (HMCs), including nesquehonite ($MgCO_3.3H_2O$), dypingite ($Mg_5(CO_3)_4(OH)_2.5H_2O$), and artinite ($Mg_2(OH)_2CO_3.3H_2O$). In most cases, nesquehonite is the most prominent Mg carbonate phase during CO_2 curing:

$$Mg(OH)_2 + CO_2 + 2H_2O \rightarrow MgCO_3 \cdot 3H_2O \quad \text{(Eq. 2)}$$

HMCs can form a well-densified structure with good binding ability, thus enhancing the mechanical properties of MC-based products [8,21]. The reaction pathways and quantitative compositions of HMCs are kinetically and thermodynamically controlled by many factors such as temperature, CO_2 pressure, ionic strength, etc [22, 23].

Accelerated carbonation of MC is well documented in the recent literature [24,25]. However, most of these studies have reported accelerated carbonation that was performed in a static CO_2

curing chamber with pressured and concentrated CO_2 gas [26,27]. This static CO_2 curing can make the maximum use of CO_2 for accelerated carbonation and facilitate the investigation of the mechanisms of MC carbonation. However, some researchers have pointed out that the static CO_2 curing represents an ideal CO_2 curing, which is an energy-intensive approach and far from practical application [28]. As the carbonation of MC is rate-limited and quite slow in an atmospheric environment, it has been argued that the re-adsorption of CO_2 from the environment will not take place to a meaningful extent in MC during its service life, meaning that the classification of "carbon negative" is doubtful [8]. The carbonation of MC and PC binary system has attracted wide attention, because the binary cement could utilise their respective advantages and alleviate individual drawbacks, achieving satisfactory carbonation efficiency, early strength, and durability [27,29]. Up to now, there is no consensus that MC and MC-based cementitious materials can be effectively carbonated to sequester CO_2 in practical situations.

In this study, we investigate the potential efficacy of accelerated carbonation of MC and MgO-based binary cement (BC) in a field-relevant situation. The flow-through CO_2 curing system can simulate a real process exhaust situation, which allows adjustable temperature, humidity, flow rate, and CO_2 concentration. The flow-through curing system can utilise CO_2-rich industrial exhaust gas as a CO_2 source for carbonation, e.g., flue gases from fossil-fuel power plants, cement rotary kilns, steelworks, and refuse incineration plants, which may contain CO_2 concentrations ranging from 5% to 20% [30]. Because the carbonation rate is sensitive to exposure conditions during CO_2 curing [31], the effects of parameters in the exhaust gas supply (CO_2 concentration, relative humidity) on carbonation of MC and BC are investigated. Additionally, exhaust CO_2 gas is usually associated with acid gases (such as SO_2 and NO_2), which should be considered before practical applications, so these contaminants are included

in the gas environment for selected experiments.

To explore the carbonation efficiency of MgO-based cement in simulated industrial exhaust gases, this study aims to: (i) assess the effect of relative humidity on the CO_2 diffusion and carbonation of MgO pastes; (ii) elucidate the influence of CO_2 concentration on the carbonation rate and formation of final carbonates; (iii) evaluate the interference of acid gases with the accelerated carbonation of MgO systems; and (iv) investigate the interactions between MC and PC in the flow-through CO_2 curing system.

2. Materials and Methodology

2.1 Materials and Sample Preparation

Reactive MgO cement and ASTM Type I ordinary Portland cement were used in this study. The MC with a density of 3.15 g cm^{-3}, produced from the calcination of $MgCO_3$ at 700 °C, was obtained from Renheng Magnesium Company, Liaoning Province, China. The PC with a density of 3.16 g cm^{-3} was purchased from Green Island Cement Limited, Hong Kong. The chemical compositions of the PC and MC cement were determined by X-ray fluorescence (XRF) and are listed in Table 1. The particle size distribution and the X-ray diffraction (XRD) data obtained for PC and MC are presented in Figure S1 and Figure S2 (Supplementary Information). Reagent-grade $Mg(NO_3)_2$, NaCl, and K_2SO_4 used for adjusting the relative humidity were purchased from Tianjin Chemical Reagent Factory, China. Reagent-grade H_2SO_4 (95-98%) and HNO_3 (70%) solution for simulating acid gases were purchased from Sigma-Aldrich.

The MC binder and a binary cement (BC) binder were investigated in the flow-through CO_2 curing condition. The BC binder was composed of 50 wt% MC and 50 wt% PC. The water-to-

binder ratio was kept at 0.25 in both cases, giving zero slump paste mixtures, which was advantageous for block production and subsequent CO_2 curing [29]. To simulate the interference of acid gases (SO_2 and NO_2), H_2SO_4 (0.125 wt% of paste) and HNO_3 (0.0137 wt% of paste) were added into specified mixtures based on theoretical calculation (in Supplementary Information). For the production of MC and BC blocks, water was added into the binder and mixed for 3 min by a planetary stirrer. The fresh pastes were cast in steel cylindrical moulds (55 mm internal diameter) and compacted with 30 MPa pressure until the height of the sample was compressed to 55 mm. After an additional 1 min compaction, the samples were demoulded immediately without slump and subjected to different curing conditions. In the flow-through CO_2 curing chamber, the relative humidity of gas was controlled at 50%, 75%, and 98% by equilibration with saturated $Mg(NO_3)_2$, NaCl, and K_2SO_4 solutions respectively; the CO_2 concentration was adjusted to 0%, 10%, 40%, 70%, and 100%; the curing times (i.e., periods of CO_2 curing) were 6 h, 1 d, 3 d, and 7 d. All experiments were conducted in triplicate and the average values are reported with error bars where appropriate. The CO_2 concentration was adjusted by controlling the blending ratio of variable flow rates of air and CO_2 gas, and a CO_2 meter (CM-0003, CO_2Meter) was used to monitor and record the CO_2 concentration in the flowing gas. A schematic diagram of the flow-through CO_2 curing set up is shown in **Figure 1**.

Table 1. Chemical compositions of PC and MC (wt %)

	Na_2O	**MgO**	**Al_2O_3**	**SiO_2**	**P_2O_5**	**SO_3**	**K_2O**	**CaO**	**Fe_2O_3**	**LOI**
PC	0.17	1.38	4.79	18.99	0.08	4.52	0.79	65.72	3.10	2.45
MC	0.00	90.46	0.46	5.81	0.10	0.10	0.15	2.22	0.59	5.42

LOI: loss on ignition; PC: ordinary Portland cement; MC: reactive MgO cement.

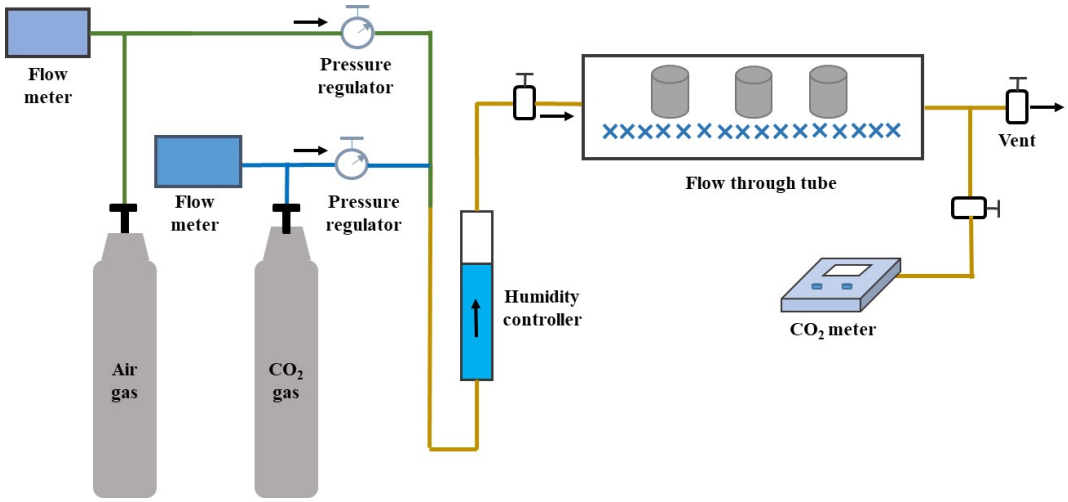

Figure 1. Schematic diagram of flow-through CO_2 curing setup.

2.2 Physical Properties and Thermogravimetric/Spectroscopic/Microscopic Analyses

The uniaxial compressive strength of the MC and BC blocks was examined by using a standard testing machine (Testometric CXM 500-50 KN) at a loading rate of 0.6 MPa s^{-1} [32]. Thermogravimetric analysis (TGA) of powder samples was performed by heating from 40°C to 1000 °C at 10 °C min^{-1} with argon purge gas (Rigaku Thermo Plus). Crystalline-phase mineralogy of samples was determined using a high-resolution powdered X-ray diffractometer (XRD, Rigaku SmartLab) in the range 2θ = 15-45° at a rate of 3° min^{-1}, with Cu Kα adiation generated at 45 kV and 200 mA. It should be noted that the XRD scan at a low angle is also important for detecting the strong peaks of hydrated magnesium carbonates in this range. For quantitative X-ray diffraction (Q-XRD) analysis, 20 wt% corundum (Al_2O_3) was used as an internal standard to determine the content of amorphous constituents, although it was regarded as a semi-quantitative method in view of the likelihood of errors. The Q-XRD analysis was calculated by the whole powder pattern fitting (WPPF) method of the integrated X-ray powder diffraction software (PDXL). The surface morphology and elemental distribution of samples with Au coating were investigated by scanning electron microscopy with energy-dispersive X-ray spectroscopy (SEM-EDX, TESCAN VEGA3 XM) at an accelerating voltage of 15 kV with

187 a current of 70-78 μA. For quality assurance, all of the samples were crushed into specified
188 size and homogeneously mixed for the analytical tests.
189
190 **3. Results and Discussion**
191 ***3.1 The Role of Relative Humidity in Hydration and Carbonation***
192 ***3.1.1 MC Pastes***
193 From the thermogravimetry (TG) curves (Figure 2a), the weight loss from 100 °C to 300 °C
194 can be ascribed to the evaporation of the physically adsorbed water and bound water from the
195 hydrated magnesium carbonates (HMCs, e.g. nesquehonite) [27]. The sharp peaks near 370 °C
196 and 390 °C in the derivative thermogravimetry (DTG) curves (Figure 2b) correspond to the
197 dehydroxylation of $Mg(OH)_2$ and decarbonisation of HMCs, respectively [27]. The mass drop
198 at higher temperatures (from 500 °C to 600 °C) was associated with the decomposition of
199 metastable Mg-carbonates. The peaks at temperatures above 600 °C mainly result from the
200 decomposition of stable, well-crystallized $MgCO_3$ [23]. In the 1-d air cured samples, there was
201 a mass loss of 12.3 wt% at 370 °C (Figure 2a), equivalent to 39.7 wt% $Mg(OH)_2$ content. The
202 air cured samples also showed 4.32 wt% mass loss due to carbonates (equivalent to 8.25 wt%
203 $MgCO_3$), which resulted from the original $MgCO_3$ in raw MgO cement (Figure S2). By
204 comparison, after 1-d CO_2 curing, the $Mg(OH)_2$ peak was reduced and shifted from 370 °C to
205 390 °C, especially in the samples with 98% humidity CO_2 curing. An obvious dehydration peak
206 of HMCs could be observed in the 98% humidity samples. Thus, 98% humidity was selected
207 as the optimal humidity for the carbonation of MC samples, although 50% humidity was
208 regarded as an optimal humidity for PC system in a previous study [16]. This is attributed to
209 the relatively high water consumption for the dissolution of $Mg(OH)_2$ ($K_{sp} = 1.13\times10^{-11}$ at 25
210 °C) compared to the $Ca(OH)_2$ ($K_{sp} = 5.02\times10^{-6}$ at 25 °C) resulting from Portland cement
211 hydration [33]. It should be noted that the content of $MgCO_3$ (approximately 10.32%) was

similar in all 1-d samples. This suggests that $Mg(OH)_2$ was preferentially carbonated into HMCs [34], because the ΔG of $MgCO_3 \cdot 3H_2O$ generation (-38.7 kJ mol^{-1}) was lower than the energy of $MgCO_3$ generation (-30.2 kJ mol^{-1}) (Figure S3).

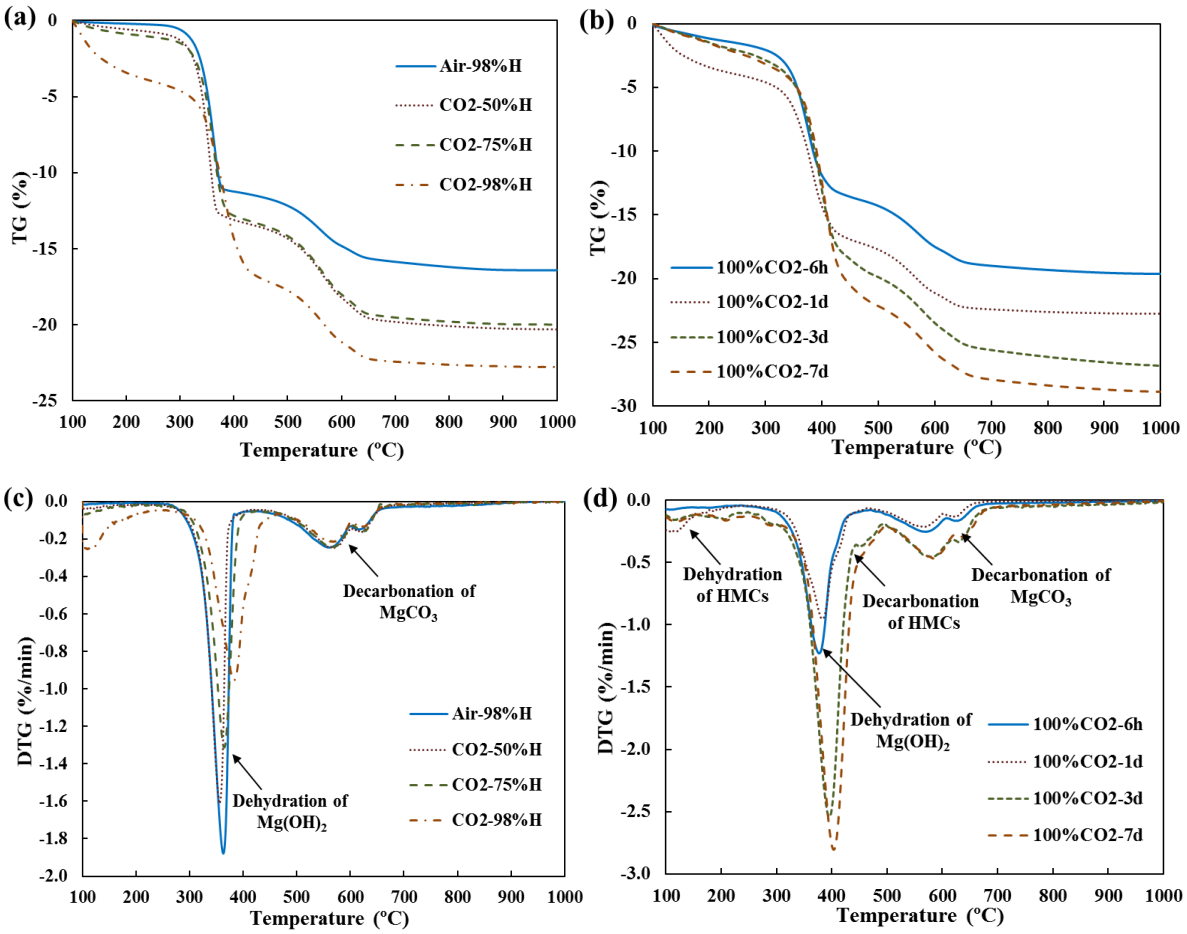

Figure 2. TGA of MC pastes: (a) TG curves of 1-d cured pastes as a function of curing environment and humidity; (b) TG curves of pastes at cured at 100% CO_2 and 98% humidity for different durations; (c) DTG curves corresponding to (a); (d) DTG curves corresponding to (b). (HMCs: hydrated magnesium carbonates).

The degree of carbonation in MC samples as a function of CO_2 curing time (at 98% humidity) is shown in Figure 2b&d. The content of newly formed HMCs in 6-h CO_2 samples was negligible, reflecting the low carbonation degree (i.e., the degree of the transformation of $Ca(OH)_2$ and $Mg(OH)_2$ into $CaCO_3$, $MgCO_3$ and HMCs) in the early term. However, after 1-d CO_2 curing, the peak at 370 °C was shifted to a higher temperature. The mass loss of HMCs

reached 11.0 wt% and 14.2 wt% in 3-d and 7-d CO_2 cured samples, respectively. Therefore, sufficient curing time is essential for continued carbonation under the flow-through curing situation where both MgO hydration and CO_2 diffusion are time-dependent processes.

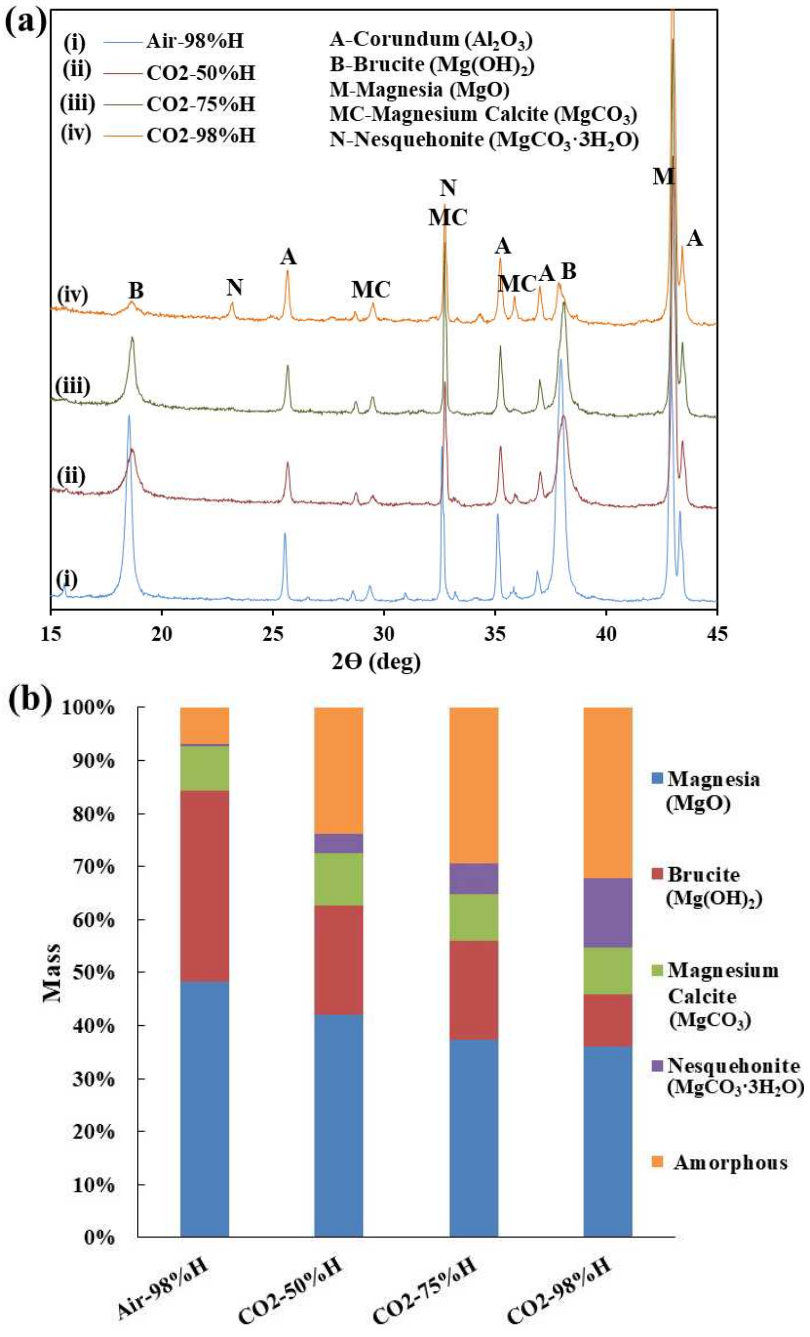

Figure 3. X-ray diffractograms (a) and Q-XRD analysis (b) of MC pastes cured for 1 day under air and CO_2 curing, with various relative humidities as marked.

237 The XRD diffractograms (Figure 3a) illustrate that a remarkable peak of brucite ($Mg(OH)_2$) at
238 18.7° 2θ existed in 1-d air cured samples. The Q-XRD results (Figure 3b) further indicate that
239 there was 36.1 wt% of $Mg(OH)_2$ content and 48.2 wt% of unreacted MgO in the air cured
240 samples. After 1-d CO_2 curing, the contents of both $Mg(OH)_2$ and MgO decreased whereas the
241 contents of $MgCO_3$, nesquehonite ($MgCO_3 \cdot 3H_2O$), and amorphous phase (e.g., poorly-
242 crystalline $Mg(OH)_2$, $MgCO_3$, and HMCs) increased, which agreed with the TGA results. In
243 particular, for the samples with 98% humidity CO_2 curing, a new peak due to nesquehonite
244 appeared at 23.2° 2θ. The XRD results provide further evidence that high relative humidity
245 (98%) is a favourable condition for CO_2 curing of MC-based materials under flow-through
246 conditions.
247
248 Figure 4 shows that MC blocks, after 6-h air curing, had a low compressive strength (3.74
249 MPa), whereas the strength reached 17.6 MPa after 1-d air curing, and gradually increased with
250 curing time due to continued MgO hydration. In the CO_2 cured samples, there was marginal
251 enhancement of strength after 6-h CO_2 curing compared to the air-cured samples. This proved
252 that 6-h curing was insufficient for CO_2 diffusion and further carbonation under the non-
253 pressurised flow-through conditions, although accelerated carbonation has previously been
254 shown to be nearly complete under higher-pressure CO_2 within 2-h of curing [34]. After 1-d
255 CO_2 curing, the compressive strength of MC samples significantly increased, and after 7-d CO_2
256 curing at 98% humidity, it was 3.8 times higher than that of the 1-d air cured samples. These
257 results demonstrate that MC pastes can be carbonated to generate abundant HMCs, as indicated
258 by the TGA and Q-XRD results (Figure 2 and 3), for strength enhancement even in the non-
259 pressurised flow-through curing system.
260

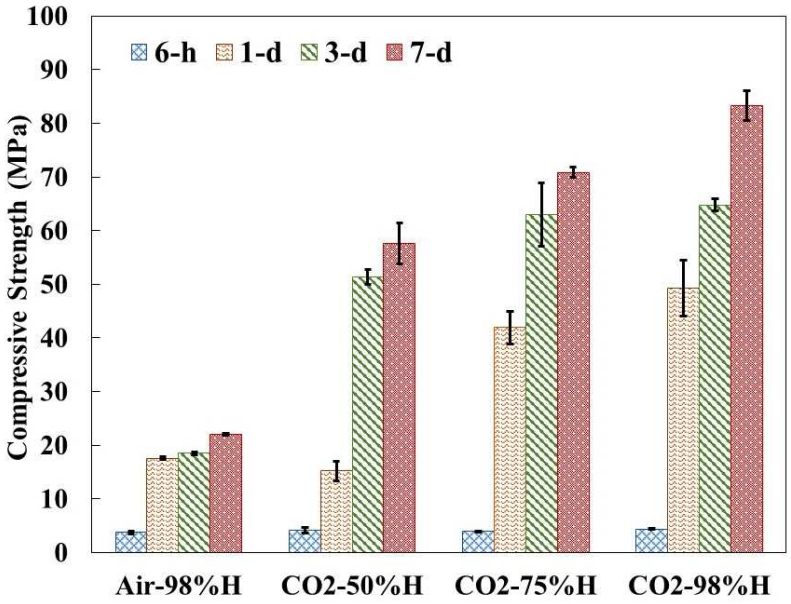

Figure 4. Compressive strength of MC pastes under air and CO_2 curing, with various relative humidities as marked.

3.1.2 BC Pastes

The TG and DTG curves of the 1-d cured BC pastes are illustrated in Figure 5a&c. From Figure 5c, 3.46 wt.% mass loss at 370 °C (equivalent to 11.7 wt.% $Mg(OH)_2$) and 1.04 wt.% mass loss at 410 °C (equivalent to 4.27 wt.% $Ca(OH)_2$) were observed in the 1-d air cured samples. By comparison, the $Ca(OH)_2$ peaks diminished and $CaCO_3$ peaks intensified after 1-d CO_2 curing, while $Mg(OH)_2$ was partially transformed into HMCs. Among the different relative humidity conditions tested, low humidity levels (50% and 75%) were favourable for the carbonation of BC pastes, which was distinct from the MC systems. In the BC system, the generation and dissolution of $Ca(OH)_2$ was much faster than $Mg(OH)_2$, thus, the CO_2 diffusion rate became the major limiting factor determining the overall rate of carbonation. As the CO_2 diffusion coefficient in water is 4 to 5 orders-of-magnitude lower than in air [35], low humidity levels (50% and 75%) facilitated CO_2 diffusion and increased the overall carbonation rate of the BC pastes.

Under 50% humidity, 6-h CO_2 curing significantly promoted the transformation from $Ca(OH)_2$ to $CaCO_3$, however, it had little effect on the carbonation of $Mg(OH)_2$. This reflects that CO_2 preferentially reacted with Ca to generate $CaCO_3$. One of the major reasons is that the ΔG of $CaCO_3$ generation (-73.0 kJ mol^{-1}) is lower than that of $MgCO_3$ generation (-30.2 kJ mol^{-1}) [34]. In addition, the dissolution and hydration of tricalcium silicate (C_3S) was much faster than that of reactive MgO in the BC system, thus the $Ca(OH)_2$ content was higher than the $Mg(OH)_2$ content at early age. After the consumption of $Ca(OH)_2$, $Mg(OH)_2$ was partially carbonated into HMCs after 1-d CO_2 curing, and then $Mg(OH)_2$ and HMCs were gradually transformed into $MgCO_3$, yet the content of hydrates and carbonates were similar in the 3-d and 7-d CO_2 cured samples.

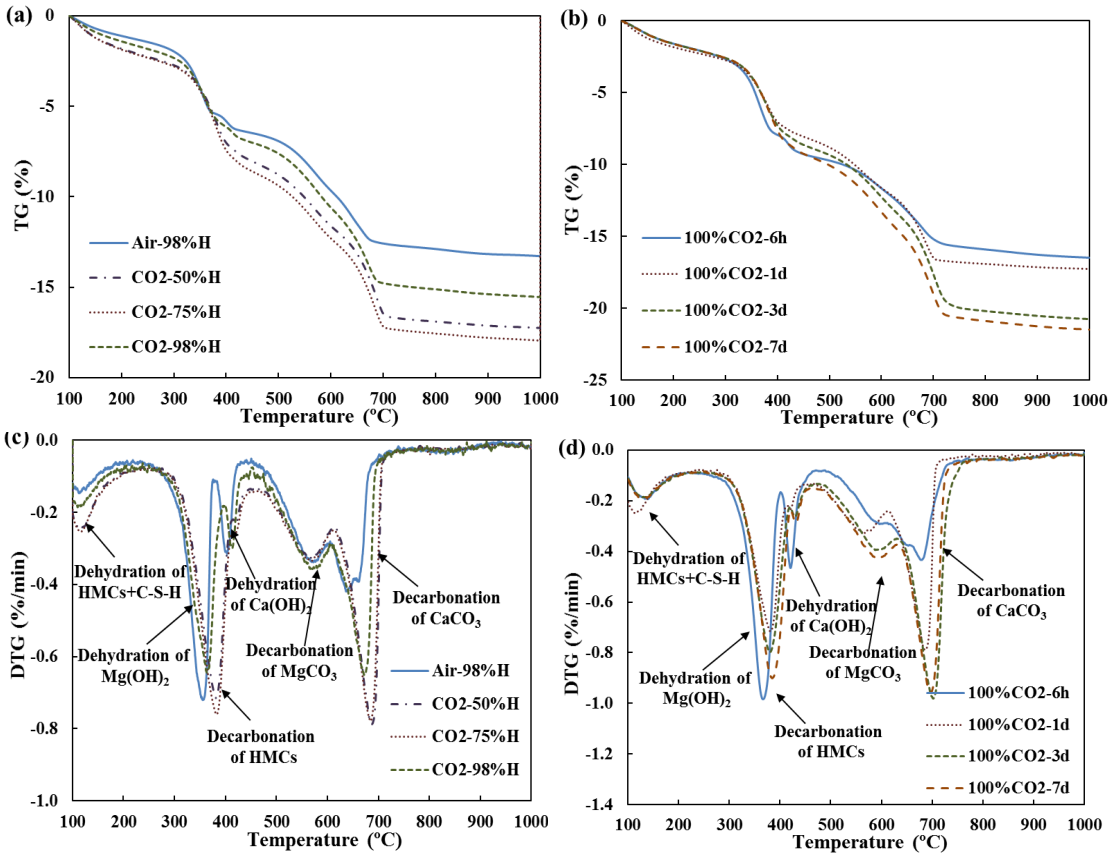

Figure 5. TGA of BC pastes: (a) TG curves of 1-d cured pastes as a function of curing environment and humidity; (b) TG curves of pastes at cured at 100% CO_2 and 50% humidity for different durations; (c) DTG curves corresponding to (a); (d) DTG curves corresponding to (b). (BC: binary cement; C-S-H: calcium silicate hydrate; HMCs: hydrated magnesium carbonates).

The Q-XRD results (Figure 6b) show that there were large quantities of unreacted MgO (34.8 wt%), C_3S (16.5 wt%), and C_2S (11.2 wt%) in the 1-d air cured samples. The 1-d CO_2 curing effectively boosted the hydration and carbonation of raw materials to generate carbonates (e.g., $CaCO_3$). The Q-XRD results confirm that $Ca(OH)_2$ was preferentially carbonated during 1-d CO_2 curing. In the early stage (1-d), the BC samples with 50% humidity CO_2 curing showed the highest carbonation degree.

As shown in Figure 7, the compressive strength of BC blocks under 6-h air curing was only 0.67 MPa, while 6-h CO_2 curing enhanced the strength to 4.03 MPa. The carbonation rate in the BC system was faster than in MC system due to the higher activity of Ca^{2+} in BC. After 1-d CO_2 curing, all the carbonated samples were stronger than the 7-d air cured samples. The strength of BC samples reached as high as 61.5 MPa after 7-d CO_2 curing. Among the samples, 50% humidity facilitated the early strength development of BC samples by accelerated carbonation whereas 98% humidity promoted the later stage (7-d) strength development by continued hydration and carbonation. Humidity as a key factor determining the rate of carbonation can be adjusted at different stages of curing under the flow-through conditions tested here, providing an interesting route to practical process optimisation.

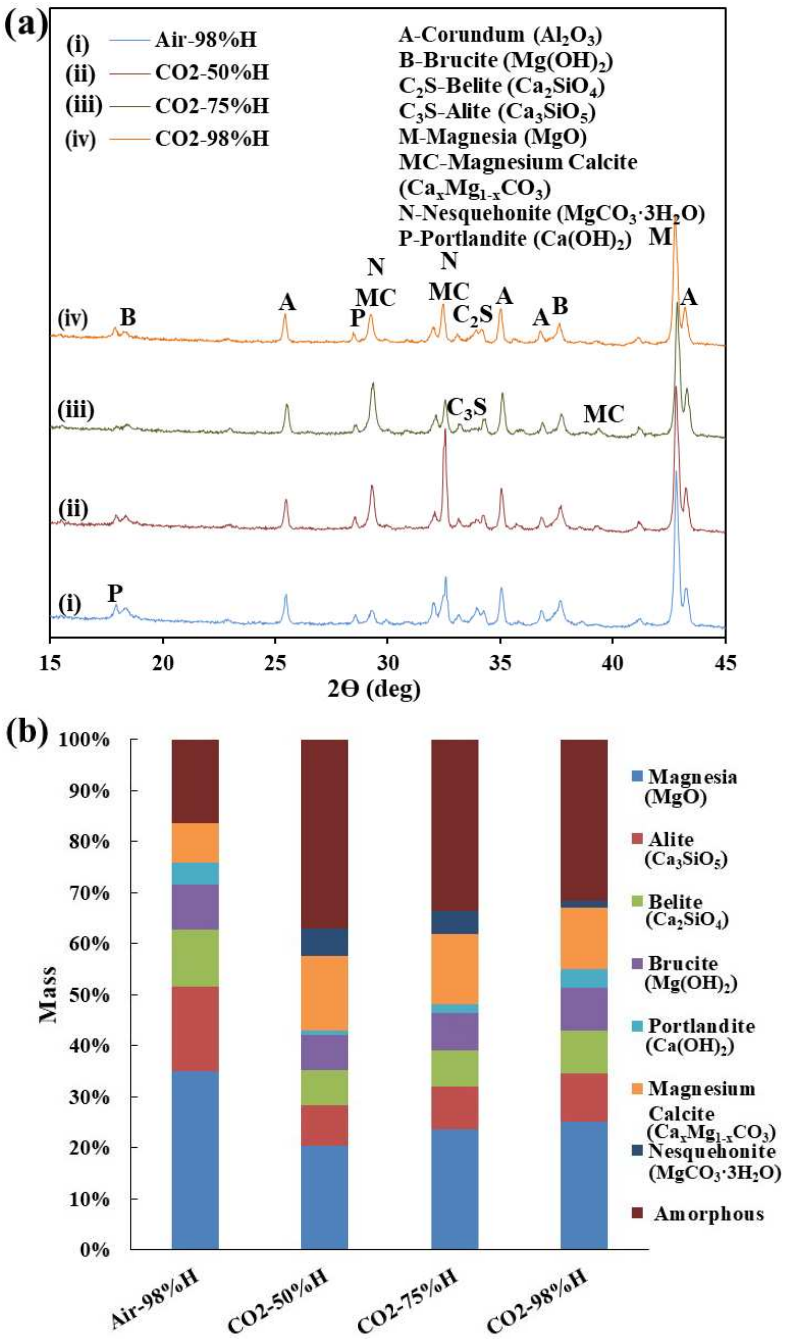

315

316

317 **Figure 6.** XRD diffractograms (a) and Q-XRD analysis (b) of 1-d cured BC pastes with

318 different humidities

319

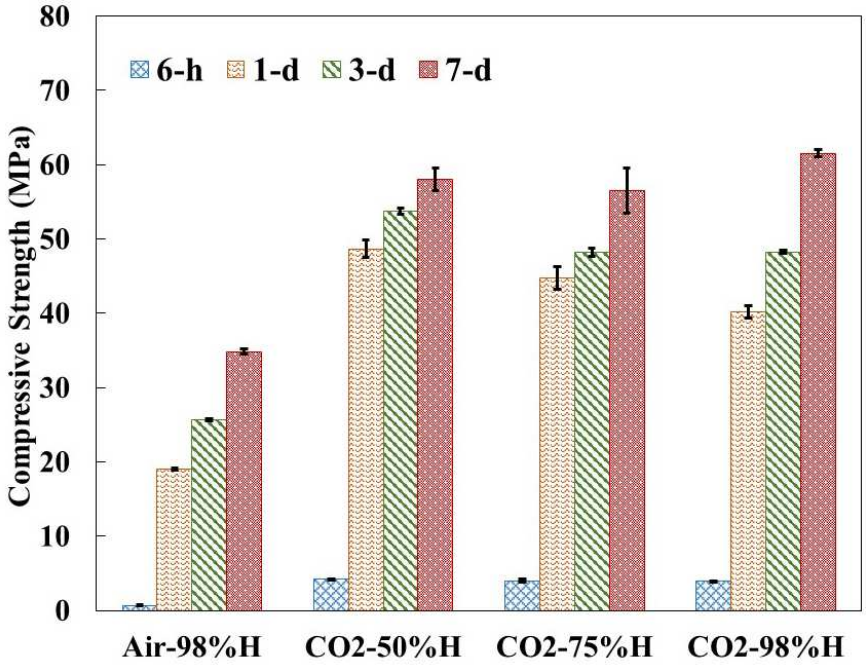

Figure 7. Compressive strengths of BC pastes under air and CO_2 curing with various humidities.

3.2 Efficiency of Various CO_2 Concentrations in Accelerated Carbonation

3.2.1 MC Pastes

As illustrated by the measured TG curves (Figure 8), the mass loss of all the carbonated samples was larger than the values for corresponding air cured samples (0% CO_2). After 1-d CO_2 curing, samples that had been subjected to different CO_2 concentrations showed similar weight drops in TG due to decarbonation at 570 ℃ (5.15 wt%) and 630 ℃ (1.30 wt%). However, compared to air cured samples, the peak at 370 °C was enlarged and shifted to 390 °C, especially for 70% CO_2 and 100% CO_2 samples. The broad peak between 100 °C and 300 °C also increased in 70% CO_2 and 100% CO_2 samples. These results suggest that the transformation of $Mg(OH)_2$ into HMCs was insignificant in the low CO_2 concentration (10% and 40%) samples while it was remarkable in the high CO_2 concentration (70% and 100%) samples. The degree of carbonation in 10% CO_2 samples increased with curing time (Figure 8b). Compared to 1-d CO_2 curing, the mass loss peak shifted from 370 °C to 390 °C after 3-d CO_2 curing (Figure 8d). The total weight drop of 7-d 10% CO_2 cured samples (22.8 wt%) was comparable to that of 1-d

100% CO_2 cured samples (22.7 wt%) (Figure 8b). Therefore, a relatively low concentration of CO_2 (e.g., 10%) under the flow-through curing conditions could still accelerate the carbonation of MC samples, and extended CO_2 curing effectively enhanced the carbonation degree.

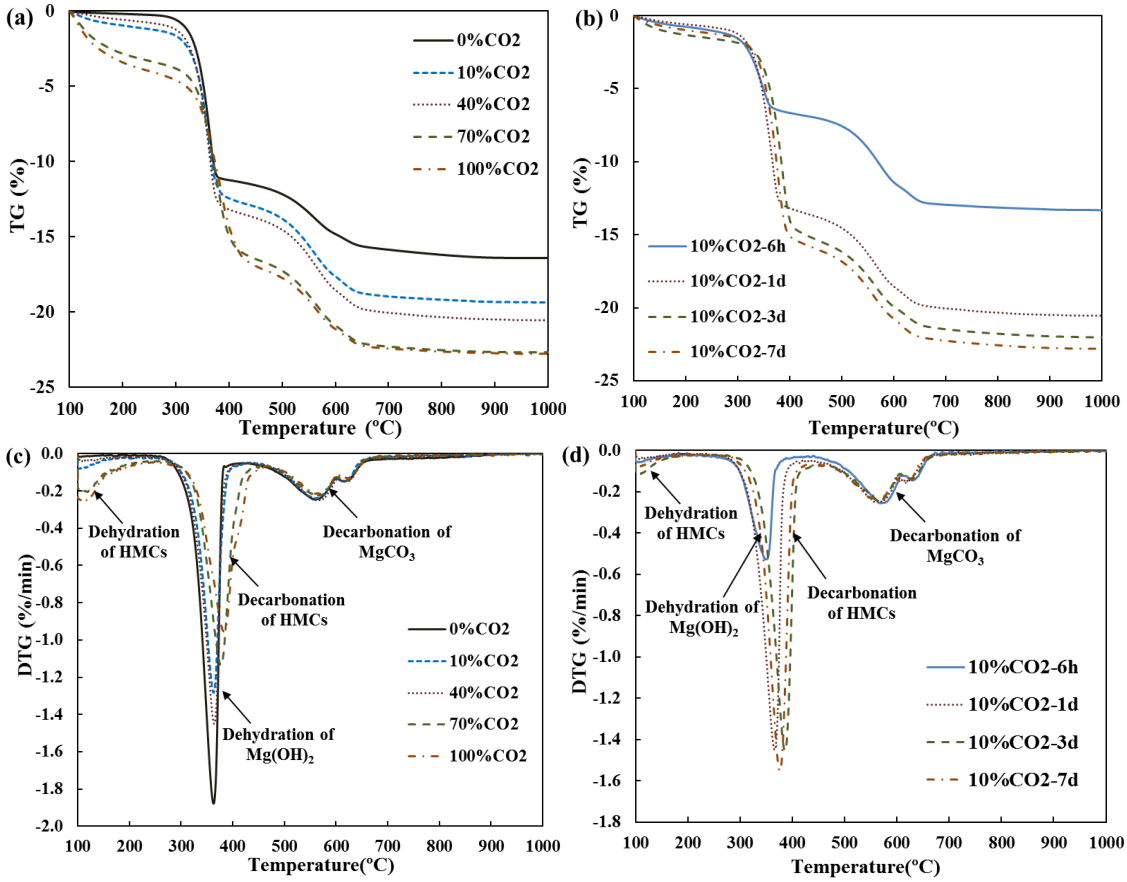

Figure 8. TGA of MC pastes: (a) TG curves of 1-d pastes as a function of CO_2 concentrations; (b) TG curves of pastes at cured at 10% CO_2 for different durations; (c) DTG curves corresponding to (a); (d) DTG curves corresponding to (b).

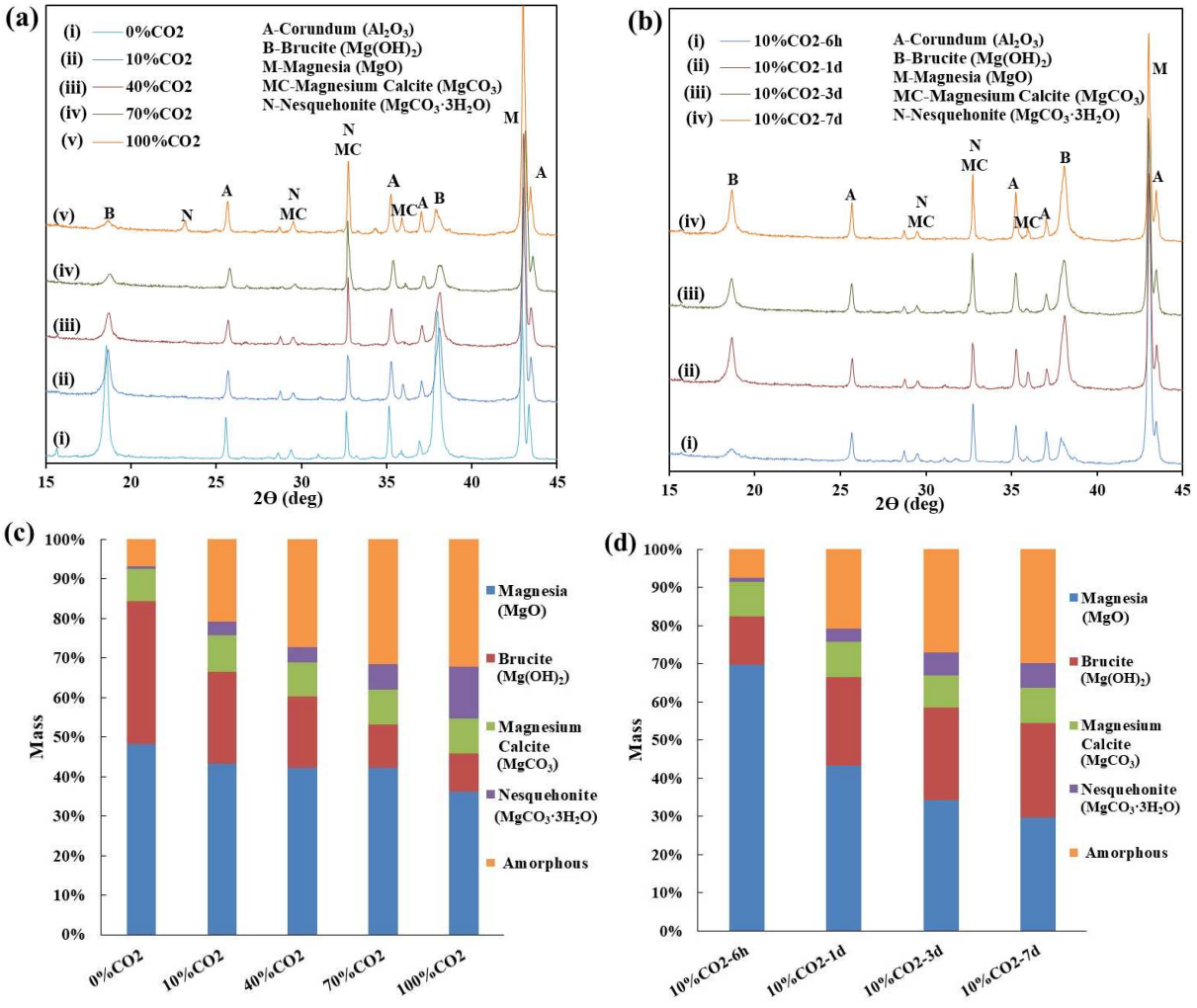

Figure 9. XRD diffractograms and Q-XRD analysis of MC pastes with different CO_2 concentrations and curing time: (a) XRD diffractograms of 1-d cured pastes with different CO_2 concentrations; (b) XRD diffractograms of pastes cured at 10% CO_2 concentration with different curing times; (c) Q-XRD analysis of 1-d cured pastes with different CO_2 concentrations; (d) Q-XRD analysis of pastes cured at 10% CO_2 concentration with different curing times.

Figure 9a illustrates that the XRD peak due to $Mg(OH)_2$ at 18.7° 2θ gradually decreased with increasing CO_2 concentration, whereas the content of $MgCO_3$ increased. In samples exposed to 100% CO_2, the peaks of nesquehonite appeared at 23.4° and 34.5° 2θ. The Q-XRD results further suggested that a high content of amorphous phase (approximately 31.2%) existed in 70% and 100% CO_2 cured samples, and HMCs were the dominant components of amorphous phase based on the TGA results. From Figure 9b&d, the content of $MgCO_3$ and amorphous HMCs in 10% CO_2 samples continually increased with curing time. The amorphous content

reached 30.2% after 7-d curing at 10% CO_2, which is further evidence that low-concentration CO_2 and sufficient curing time can still promote carbonation of MC products.

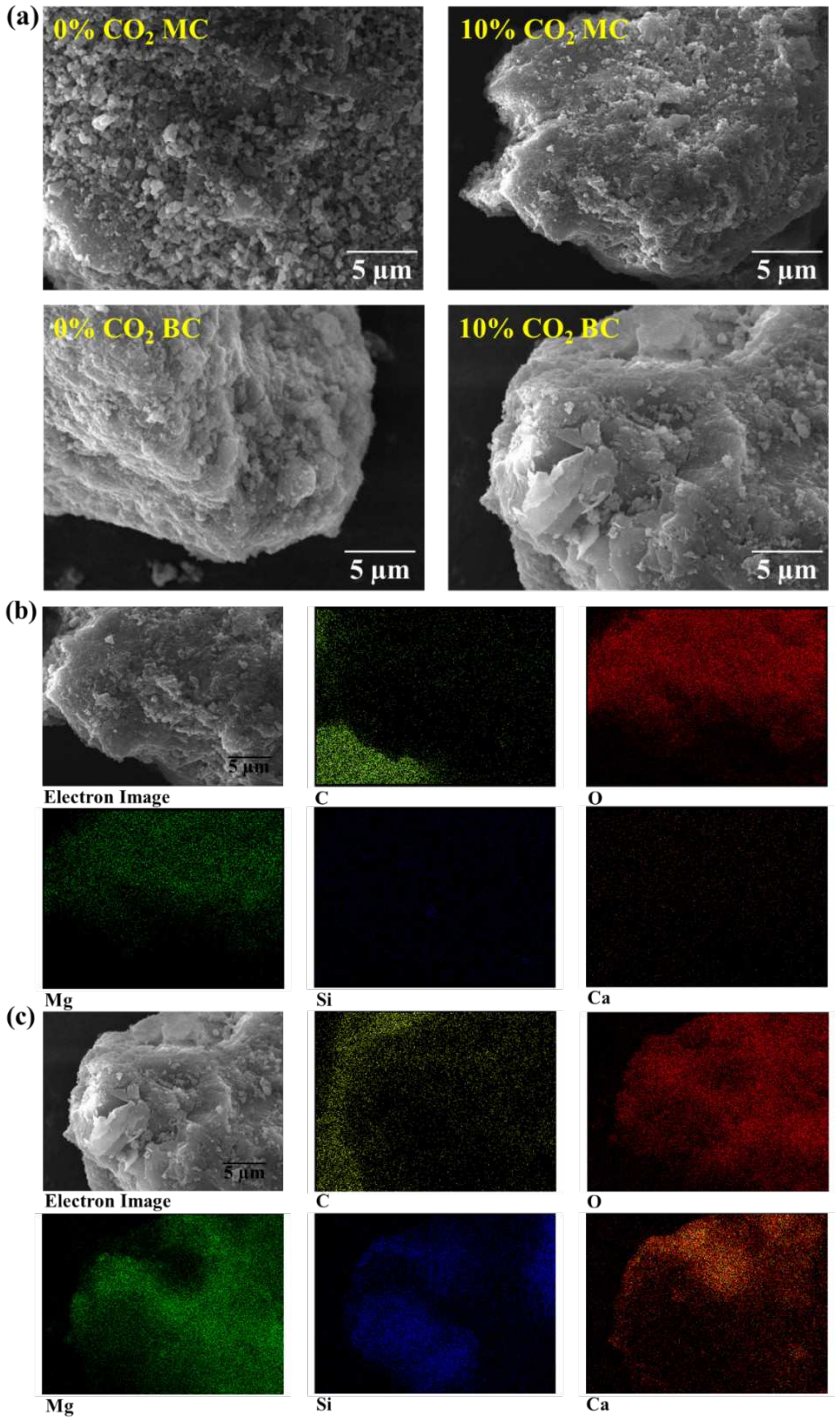

Figure 10. SEM images and elemental mapping of MC and BC samples: (a) SEM image of 1-d 0% CO_2 and 10% CO_2 cured MC and BC samples, (b) element mapping of 1-d 10% CO_2 cured MC samples, (c) element mapping of 1-d 10% CO_2 cured BC samples.

As illustrated in SEM images (Figure 10a), 1-d air (0% CO_2) cured MC samples had a rough surface with a large number of spherical particles, which may be unreacted MgO particles [36]. By comparison, 1-d 10% CO_2 cured MC samples showed a dense structure, suggesting favourable MC hydration and carbonation. Elemental mapping (Figure 10b) showed that Mg and O were the predominant elements and only a low content of C existed in 1-d 10% CO_2 cured samples. Therefore, under low-concentration CO_2 curing conditions, a long time CO_2 curing is required to achieve a high degree of carbonation.

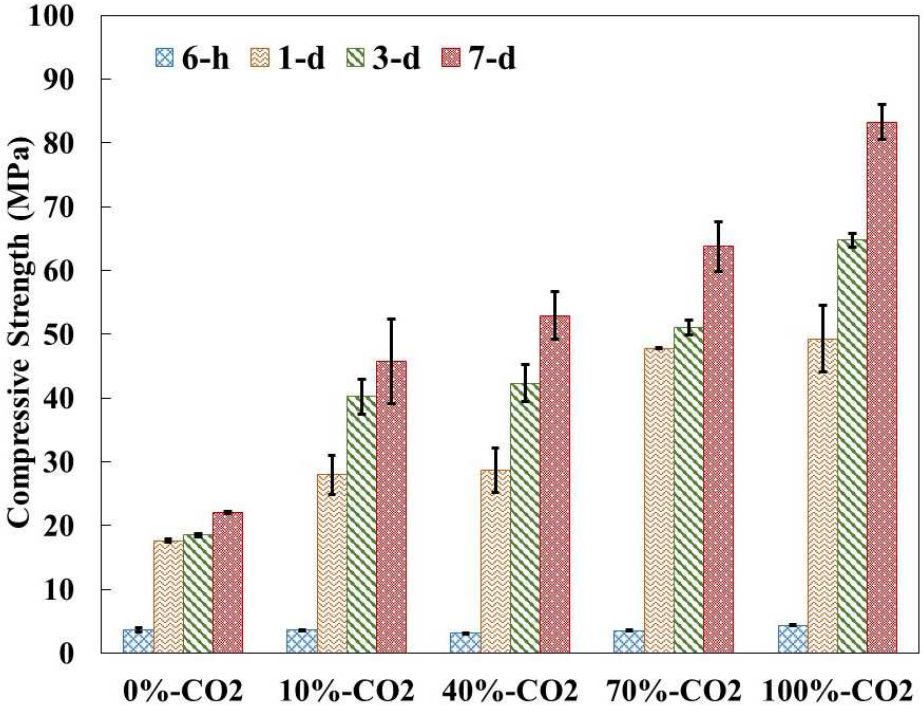

Figure 11. Compressive strengths of MC pastes under CO_2 curing with various CO_2 concentrations.

Figure 11 shows that after 6-h CO_2 curing, all the MC blocks showed comparable compressive strengths (3.74-4.41 MPa). After 1-d CO_2 curing, the differences in compressive strength were significant among different CO_2 cured samples. The 1-d 10% CO_2 cured samples showed higher strength than 7-d air cured samples, and strength increased with the increase of CO_2

concentration because of the favourable carbonation as indicated by the TGA and Q-XRD results (Figure 8 and 9). It should be noted that extended 10% CO_2 curing (7-d) yielded similar strengths to 1-d 100% CO_2 cured samples. These findings demonstrate that a low CO_2 concentration gas (e.g., industrial exhaust) could be used to accelerate carbonation of MC-based materials, although it needs a relatively long curing time compared to 100% CO_2 curing.

3.2.2 BC Pastes

Figure 12a illustrates that the mass loss of 1-d carbonated BC samples increased with an increase of CO_2 concentration, and that the $Ca(OH)_2$ in BC systems was preferentially carbonated into $CaCO_3$. The obvious peaks of $Ca(OH)_2$ could be observed for the lower-CO_2 cured samples, whereas $Ca(OH)_2$ peaks nearly disappeared and $Mg(OH)_2$ was partially transformed into HMCs and $MgCO_3$ in 100% CO_2 cured samples (Figure 12c). The contents of carbonates increased with CO_2 curing time. The extent of calcite decomposition measured by TG for 10%-CO_2 cured samples increased from 4.8 wt% (6-h curing) to 9.0 wt% (7-d curing). The peak of $Mg(OH)_2$ (370 °C) was also shifted to a temperature indicative of HMCs (390 °C) after 7-d CO_2 curing (Figure 12d). Thus, long-term curing at low concentration CO_2 curing could also accelerate the carbonation of BC.

As shown in Figure 13a&c, with the increase of CO_2 concentration the content of $Ca(OH)_2$ in 1-d cured BC samples gradually decreased, however, $Mg(OH)_2$ content was maintained at approximately 8.6%, except in 100% CO_2 cured samples, suggesting that only $Ca(OH)_2$ was partially carbonated in the early stages. From Figure 13b&d, the contents of $Ca(OH)_2$ and $Mg(OH)_2$ in 10% CO_2 cured samples continually decreased with increasing curing time, while the contents of calcite and amorphous phase accordingly increased. After 7-d curing at 10% CO_2, the contents of calcite and amorphous phase (C-S-H, calcium aluminate hydrates,

amorphous HMCs, poorly crystalline carbonates, etc.) reached 13.5% and 36.9%, respectively, which were also comparable to the contents of these phases in 1-d 100% CO_2 cured BC samples.

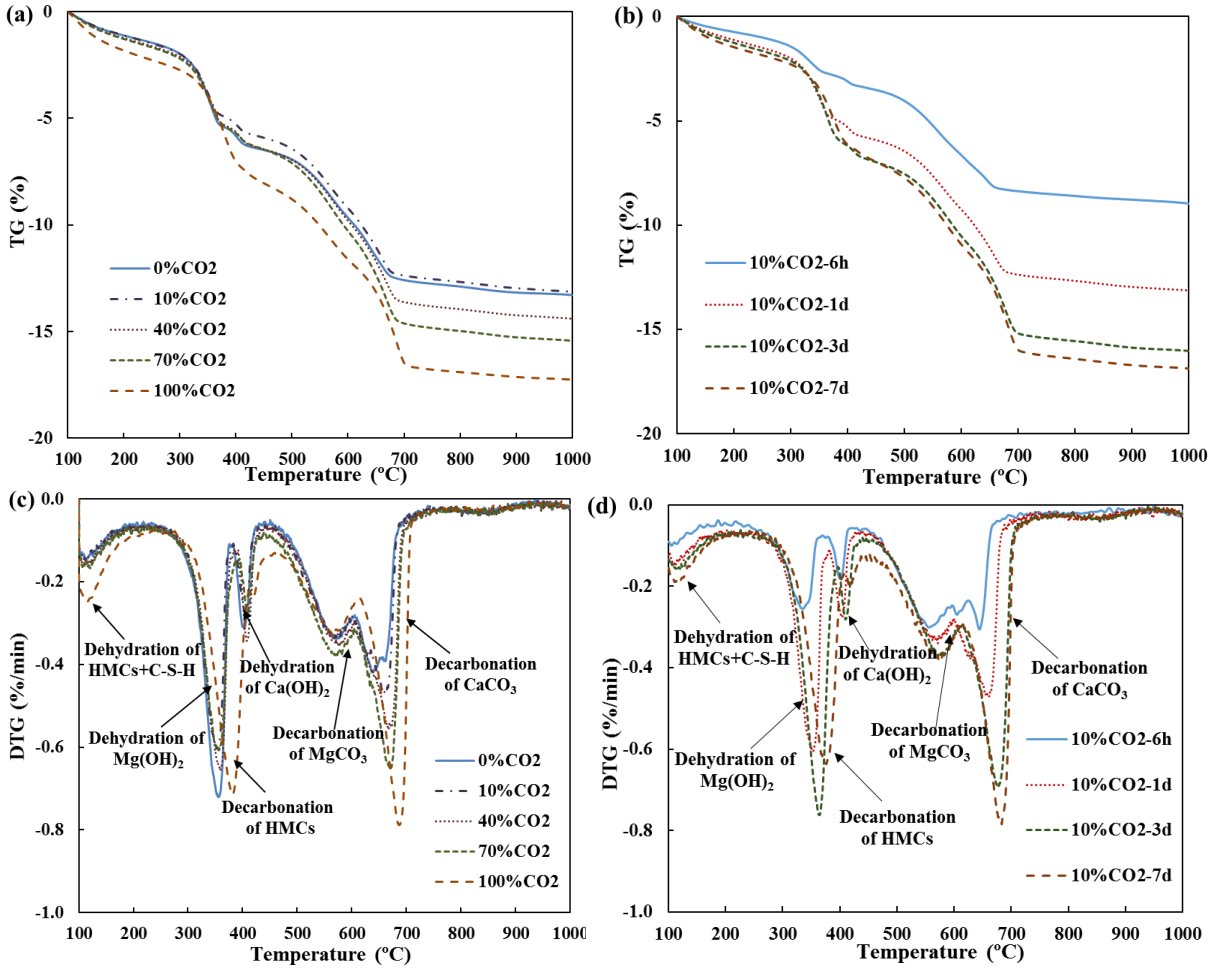

Figure 12. TGA of BC pastes: (a) TG curves of 1-d pastes as a function of CO_2 concentrations; (b) TG curves of pastes at cured at 10% CO_2 for different durations; (c) DTG curves corresponding to (a); (d) DTG curves corresponding to (b).

From SEM imaging (Figure 10a), 1-d air cured BC samples had a rough surface but the spherical particles on the surface were not remarkable. In contrast to the MC samples, most of MgO particles in the BC samples might be enclosed by PC hydrates (e.g., C-S-H gel) [37]. After 1-d 10% CO_2 curing, a smooth and dense surface could be observed for BC samples. Elemental mapping (Figure 10c) illustrated that 1-d 10% CO_2 cured BC samples have a higher

content of carbon than the corresponding MC samples, and the carbon overlapped with the Ca-rich areas. This provides further evidence that CO_2 reacted with Ca^{2+} preferentially due to the relatively high solubility and reactivity of $Ca(OH)_2$. Therefore, the PC in the BC system played an important role in promoting the early-term carbonation in low-CO_2 concentration condition.

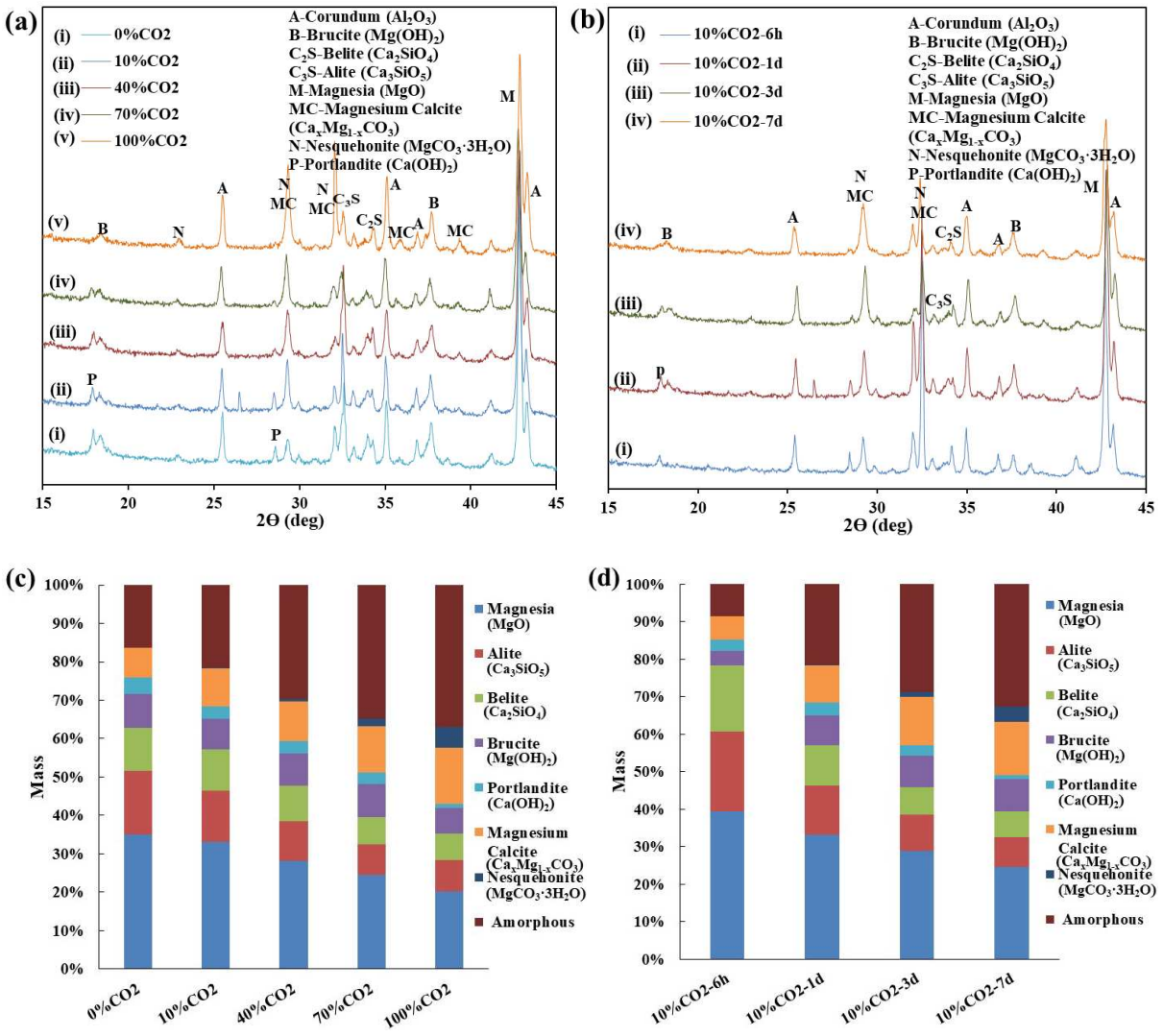

Figure 13. XRD diffractograms and Q-XRD analysis of BC pastes with different CO_2 concentrations and curing times: (a) XRD diffractograms of 1-d cured pastes with different CO_2 concentrations; (b) XRD diffractograms of pastes cured at 10% CO_2 concentration with different curing times; (c) Q-XRD analysis of 1-d cured pastes with different CO_2 concentrations; (d) Q-XRD analysis of pastes cured at 10% CO_2 concentration with different curing times.

As shown in Figure 14, BC samples with high-concentration CO_2 curing presented higher

compressive strengths at different curing durations due to their higher carbonation rate. However, the lower CO_2 concentration curing still effectively accelerated carbonation. Compared to 7-d air cured samples, the 7-d 10% CO_2 cured samples showed 31.8% enhancement of compressive strength, which gave comparable strength with 1-d 100% CO_2 cured samples. Therefore, low CO_2 concentration gas under flow-through conditions is also effective for accelerating the carbonation of BC-based materials.

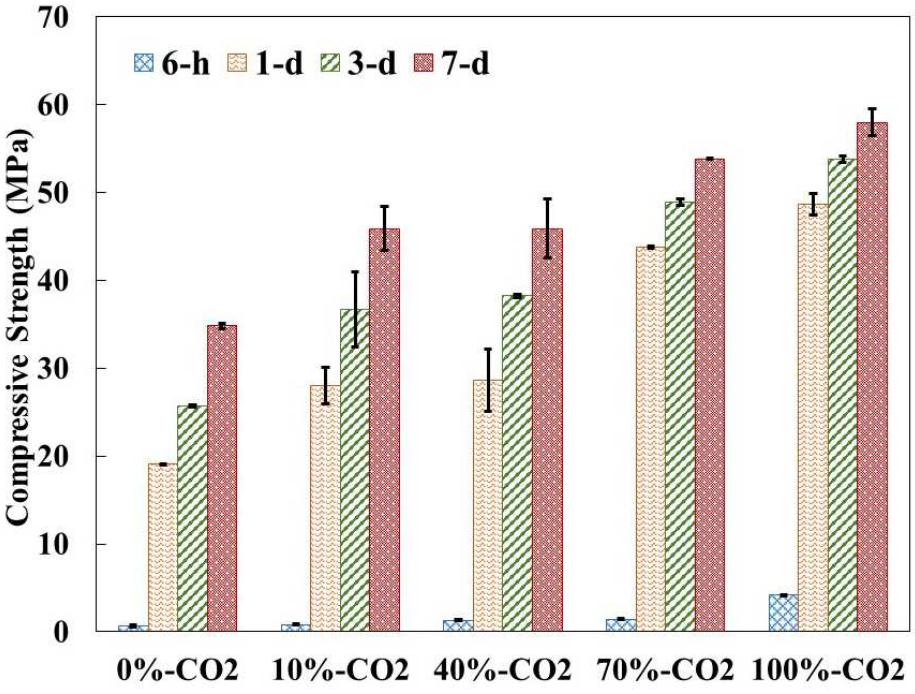

Figure 14. Compressive strength of BC pastes cured under CO_2 with various CO_2 concentrations.

3.3 Effect of Acids on Accelerated Carbonation

The TG results (Figure 15) indicate that the mass loss of hydrates and carbonates of 1-d CO_2 cured MC samples significantly reduced in the presence of H_2SO_4 and HNO_3 as representative acids that may be observed in flue gases. The carbonation of the MC samples was significantly inhibited by the acidic conditions. As the acidities of H_2SO_4 and HNO_3 are stronger than H_2CO_3, carbonates could not displace SO_4^{2-} and NO_3^- from the MC samples as the stronger acids reacted preferentially with the solid alkaline phases [38]. The sulphation and nitration are

irreversible processes [39]. It should be noted that the molar concentration of H_2SO_4 tested here was 5.83 times higher than the value of HNO_3 based on an investigation in power plant exhaust (in Supplementary Information). From Figure 15c, compared to acid-free MC samples, the mass loss in TG attributed to HMCs decomposition in acid-incorporated samples significantly reduced, especially for the H_2SO_4-MC samples. Thus, in actual application, a high concentration of SO_2 in the exhaust may have a remarkable inhibitive effect on MC carbonation.

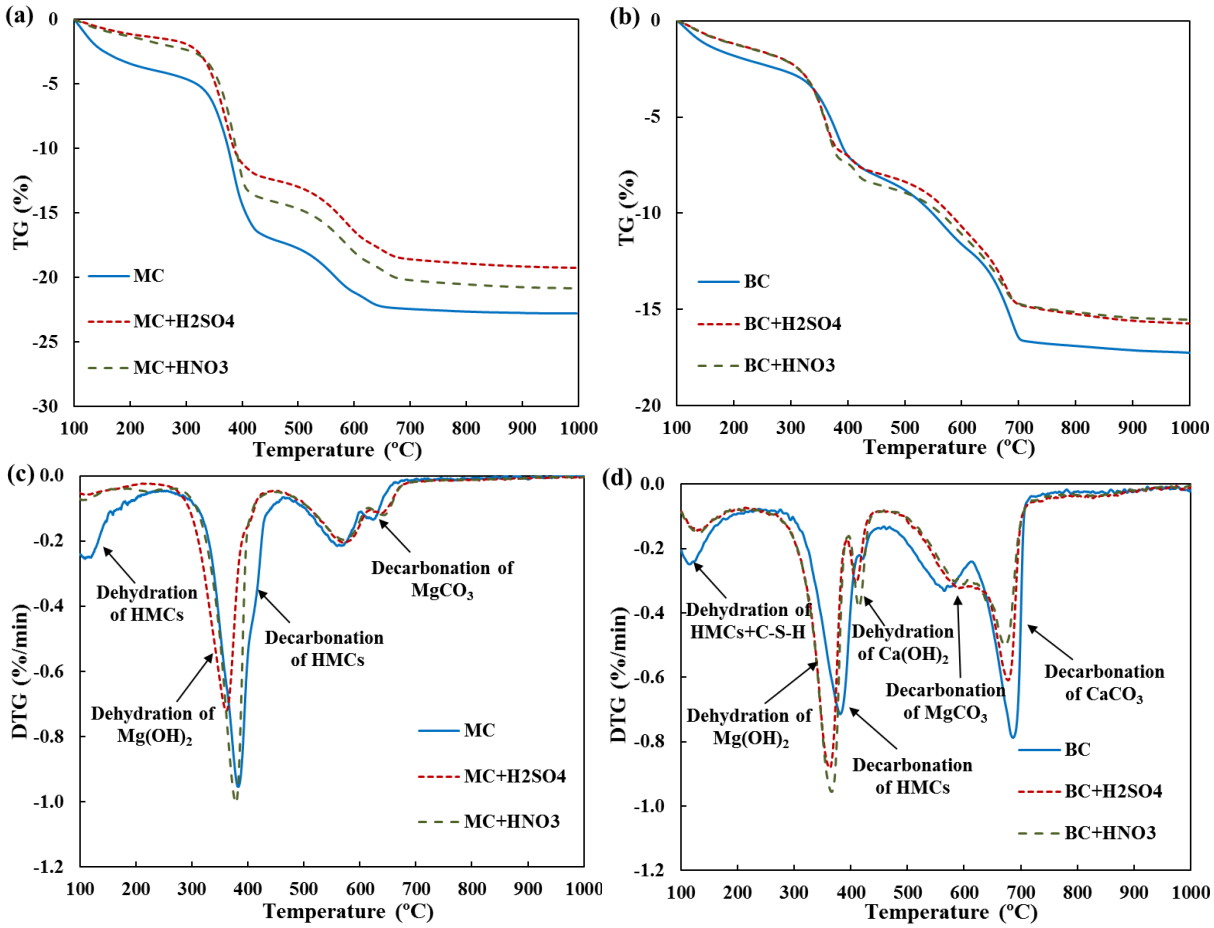

Figure 15. TGA of 1-d 100% CO_2 cured pastes with H_2SO_4 and HNO_3 addition: (a) TG curves of MC pastes with addition of acids; (b) TG curves of BC pastes with addition of acids; (c) DTG curves corresponding to (a); (d) DTG curves corresponding to (b).

In the TG analysis of the 1-d CO_2 cured BC system (Figure 15b&d), the presence of H_2SO_4 and HNO_3 resulted in an 11% reduction in the mass loss of the hydrates and carbonates, respectively, which was lower than the reduction in the MC system. This suggests that BC samples had better compatibility with acids compared to MC samples. The high concentration of H_2SO_4 and low concentration of HNO_3 had a similar inhibitory effect on carbonation in the BC system. The H_2SO_4 may react with $Ca(OH)_2$ to form $CaSO_4$, which is one of the components in PC (Table 1). Thus, PC in the BC system may to some degree be able to compensate for the adverse effect of H_2SO_4.

As shown in Figure 16, compared to acid-free CO_2 cured MC samples, the acid-incorporated samples contained a higher content of uncarbonated $Mg(OH)_2$, particularly for the H_2SO_4 samples. Q-XRD analyses further indicated that the presence of H_2SO_4 and HNO_3 reduced the content of nesquehonite by 90.3% and 84.7%, respectively, and also the amorphous content decreased. In the BC system, the acids also resulted in the increase of unreacted raw materials and decrease of carbonates and hydrates (crystalline or amorphous phases). In particular, the presence of H_2SO_4 in BC samples consumed $Ca(OH)_2$ and decreased the content of calcite.

From Figure 17, the incorporation of acids decreased the compressive strength of 1-d air cured MC samples by approximately 37.8% due to its inhibitory effect on the hydrates formation. For CO_2 cured samples, the addition of H_2SO_4 and HNO_3 led to 64.0% and 44.5% strength reduction, respectively. This suggests that acids significantly inhibited the carbonation of MC, especially for high-concentration H_2SO_4, which was in accordance with TGA and XRD results. Conversely, the incorporation of H_2SO_4 and HNO_3 showed a negligible effect on the strength reduction in the air cured BC system, but reduced the strength of CO_2 cured BC samples by

40.8% and 39.8%, respectively. Hence, compared to the MC system, the BC system had a better compatibility with acids. To ensure effective accelerated carbonation, desulphurisation and acid gas neutralisation in the exhaust gas should be considered before employing this gas as a flow-through CO_2 curing source for MC and BC systems.

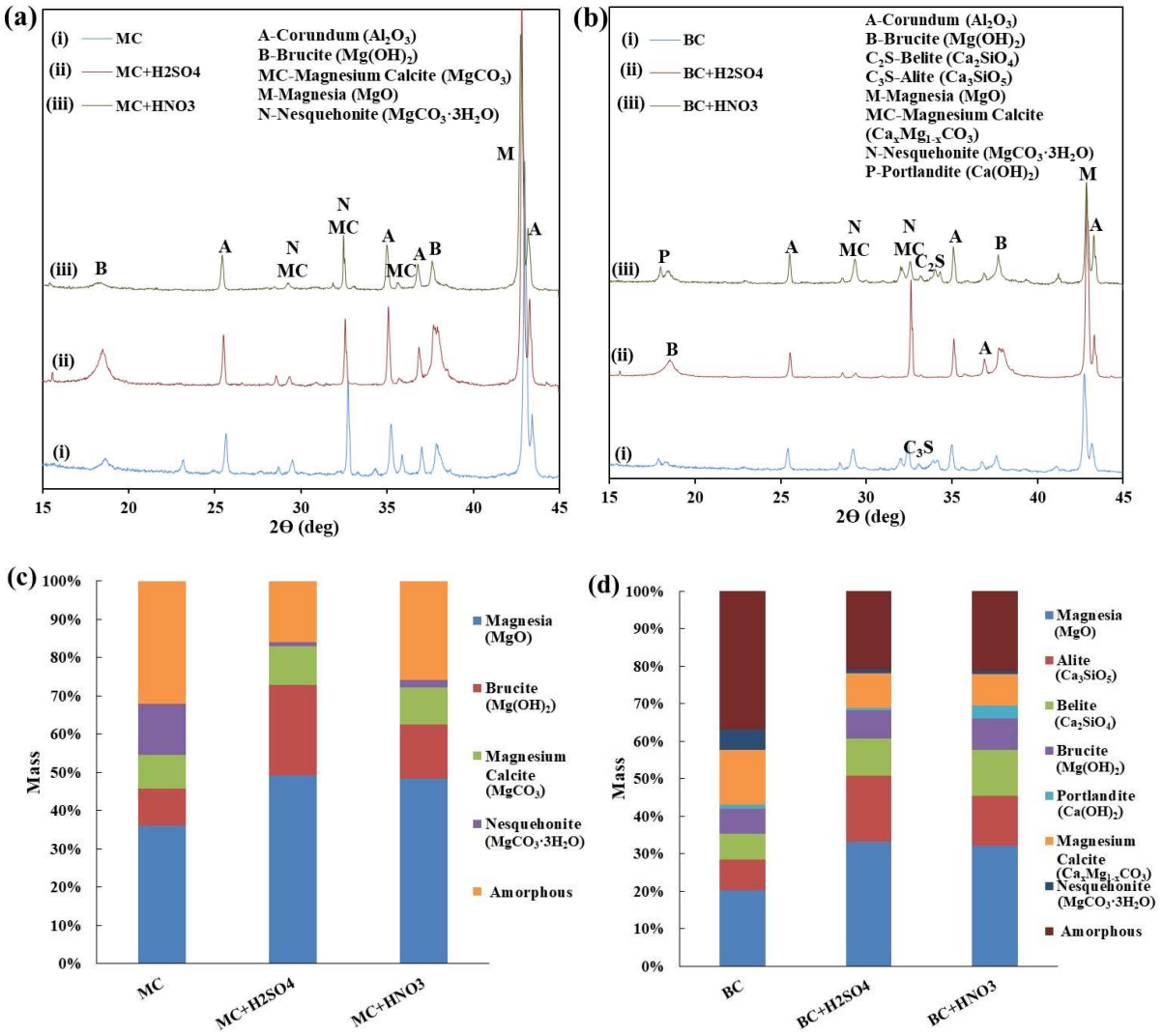

Figure 16. XRD diffractograms and Q-XRD analysis of 1-d 100% CO_2 cured pastes with H_2SO_4 and HNO_3 addition: (a) XRD diffractograms of MC pastes with addition of acids; (b) XRD diffractograms of BC pastes with addition of acids; (c) Q-XRD analysis of MC pastes with addition of acids; (d) Q-XRD analysis of BC pastes with addition of acids.

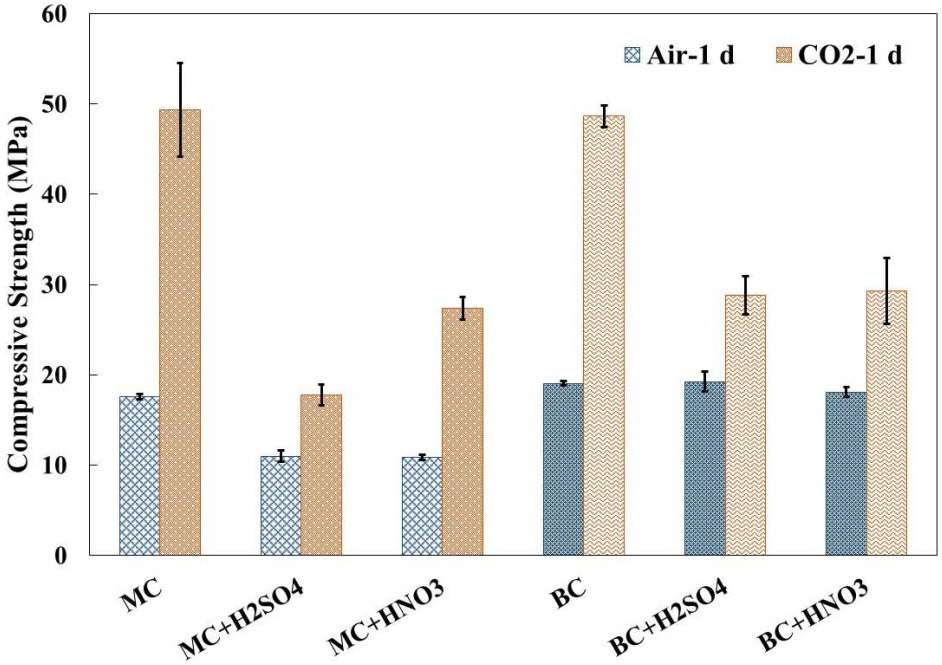

Figure 17. Compressive strengths of 1-d air and 100% CO_2 cured MC and BC samples with addition of acids.

4. Conclusions

This study investigated the accelerated carbonation of low-carbon reactive MgO cement and ordinary Portland cement blends under flow-through CO_2 gas conditions. The experimental results showed that flow-through CO_2 curing at a relatively low concentration (simulated industrial exhaust) effectively accelerated carbonation and enhanced compressive strength of single MgO cement (MC) pastes and binary cement (BC) pastes. High relative humidity (98%) was favourable for CO_2 curing of the MC system due to the high water consumption of MC for the generation and dissolution of $Mg(OH)_2$, whereas low humidity (50%) was an optimal parameter for BC paste carbonation. The addition of Portland cement (PC) into the BC system boosted early-term carbonation rate due to the rapid formation and dissolution of $Ca(OH)_2$. Despite the lower carbonation rate at 10% CO_2 concentration, the carbonation degree and compressive strength of 7-d 10% CO_2 cured samples were comparable to the values obtained for 1-d 100% CO_2 cured samples. Nevertheless, the presence of acids replicating the acid gases in industrial exhausts had inhibitory effects on the carbonation and hydration of MC pastes. By

532 comparison, the PC included in the BC system have a better compatibility with SO_4^{2-} and partly
533 relieved the inhibitory effect. In future studies, the effect of NO_2 and SO_2 from the exhaust gas
534 on the carbonation and hydration of cement-based materials should be further evaluated, and
535 the flow-through curing system should be optimised to enhance the recovery rate of CO_2 from
536 the exhaust gas. Overall, this study demonstrated that low-carbon MgO-based cement can be a
537 promising material for sequestering and utilising CO_2 from industrial exhausts to promote the
538 development of negative-emission technologies.
539

540 **Acknowledgement**

541 The authors appreciate the financial support from the Hong Kong Research Grants Council
542 (PolyU 15223517 and E-PolyU503/17) for this study.
543

544 **References**

545 [1] K.L. Scrivener, V.M. John, E.M. Gartner, Eco-efficient cements: Potential economically
546 viable solutions for a low-CO_2 cement-based materials industry, Cem. Concr. Res. 114 (2018)
547 2–26.
548 [2] N.T. Dung, C. Unluer, Development of MgO concrete with enhanced hydration and
549 carbonation mechanisms, Cem. Concr. Res. 103 (2018) 160–169.
550 [3] Y. Geng, Z. Wang, L. Shen, J. Zhao, Calculating of CO_2 emission factors for Chinese
551 cement production based on inorganic carbon and organic carbon, J. Clean. Prod. 217 (2019)
552 503–509.
553 [4] L. Wang, K. Yu, J.S. Li, D.C.W. Tsang, C.S. Poon, J.C. Yoo, K. Baek, S. Ding, D. Hou,
554 J.G. Dai, Low-carbon and low-alkalinity stabilization/solidification of high-Pb contaminated
555 soil, Chem. Eng. J. 351 (2018) 418–427.

[5] A. Al-Tabbaa, Reactive magnesia cement, in: Eco-Efficient Concrete. Woodhead Publishing (2013) 523–543.

[6] T. Zhang, X. Liang, C. Li, M. Lorin, Y. Li, L.J. Vandeperre, C.R. Cheeseman, Control of drying shrinkage in magnesium silicate hydrate (M-S-H) gel mortars, Cem. Concr. Res. 88 (2016) 36–42.

[7] H. Dong, E.H. Yang, C. Unluer, F. Jin, A. Al-Tabbaa, Investigation of the properties of MgO recovered from reject brine obtained from desalination plants, J. Clean. Prod. 196 (2018) 100–108.

[8] S.A. Walling, J.L. Provis, Magnesia-Based Cements: A Journey of 150 Years, and Cements for the Future?, Chem. Rev. 116 (2016) 4170–4204.

[9] Y. Tan, H. Yu, Y. Li, W. Bi, X. Yao, The effect of slag on the properties of magnesium potassium phosphate cement, Constr. Build. Mater. 126 (2016) 313–320.

[10] L. Wang, L. Chen, D.W. Cho, D.C.W. Tsang, J. Yang, D. Hou, K. Baek, H.W. Kua, C.S. Poon, Novel synergy of Si-rich minerals and reactive MgO for stabilisation/solidification of contaminated sediment, J. Hazard. Mater. 365 (2019) 695–706.

[11] L. Wang, L. Chen, D.C.W. Tsang, H.W. Kua, J. Yang, Y.S. Ok, S.M. Ding, D.Y. Hou, C.S. Poon, The roles of biochar as green admixture for sediment-based construction products. Cem. Concr. Compos. 104 (2019) 103348.

[12] C. Kuenzel, F. Zhang, V. Ferrándiz-Mas, C.R. Cheeseman, E.M. Gartner, The mechanism of hydration of MgO-hydromagnesite blends, Cem. Concr. Res. 103 (2018) 123–129.

[13] L. Wang, I.K.M. Yu, D.C.W. Tsang, K. Yu, S. Li, C. Sun Poon, J.G. Dai, Upcycling wood waste into fibre-reinforced magnesium phosphate cement particleboards, Constr. Build. Mater. 159 (2018) 54–63.

579 [14] L. Mo, F. Zhang, M. Deng, F. Jin, A. Al-Tabbaa, A. Wang, Accelerated carbonation and
580 performance of concrete made with steel slag as binding materials and aggregates, Cem. Concr.
581 Compos. 83 (2017) 138–145.
582 [15] F. Cao, M. Miao, P. Yan, Hydration characteristics and expansive mechanism of MgO
583 expansive agents, Constr. Build. Mater. 183 (2018) 234–242.
584 [16] B.J. Zhan, D.X. Xuan, C.S. Poon, C.J. Shi, Effect of curing parameters on CO_2 curing of
585 concrete blocks containing recycled aggregates, Cem. Concr. Compos. 71 (2016) 122–130.
586 [17] C. Shi, Z. Wu, Z. Cao, T.C. Ling, J. Zheng, Performance of mortar prepared with recycled
587 concrete aggregate enhanced by CO_2 and pozzolan slurry, Cem. Concr. Compos. 86 (2018)
588 130–138.
589 [18] N.T. Dung, C. Unluer, Carbonated MgO concrete with improved performance: The
590 influence of temperature and hydration agent on hydration, carbonation and strength gain,
591 Cem. Concr. Compos. 82 (2017) 152–164.
592 [19] S.A. Walling, J.L. Provis, A discussion of the papers “Impact of hydrated magnesium
593 carbonate additives on the carbonation of reactive MgO cements” and “Enhancing the
594 carbonation of MgO cement porous blocks through improved curing conditions”, by C. Unluer
595 & A. Al-Tabbaa, Cem. Concr. Res. 79 (2016) 424–426.
596 [20] M. Fernández Bertos, S.J.R. Simons, C.D. Hills, P.J. Carey, A review of accelerated
597 carbonation technology in the treatment of cement-based materials and sequestration of CO_2.,
598 J. Hazard. Mater. 112 (2004) 193–205.
599 [22] L. Mo, F. Zhang, D.K. Panesar, M. Deng, Development of low-carbon cementitious
600 materials via carbonating Portland cement–fly ash–magnesia blends under various curing
601 scenarios: a comparative study, J. Clean. Prod. 163 (2017) 252–261.
602 [21] L. Pu, C. Unluer, Durability of carbonated MgO concrete containing fly ash and ground
603 granulated blast-furnace slag, Constr. Build. Mater. 192 (2018) 403–415.

604 [23] L. Mo, D.K. Panesar, Effects of accelerated carbonation on the microstructure of Portland
605 cement pastes containing reactive MgO, Cem. Concr. Res. 42 (2012) 769–777.
606 [24] S. Ruan, C. Unluer, Influence of mix design on the carbonation, mechanical properties
607 and microstructure of reactive MgO cement-based concrete, Cem. Concr. Compos. 80 (2017)
608 104–114.
609 [25] R. Zhang, D.K. Panesar, Mechanical properties and rapid chloride permeability of
610 carbonated concrete containing reactive MgO, Constr. Build. Mater. 172 (2018) 77–85.
611 [26] L. Wang, S.S. Chen, D.C.W. Tsang, C.S. Poon, J.G. Dai, CO_2 curing and fibre
612 reinforcement for green recycling of contaminated wood into high-performance cement-
613 bonded particleboards, J. CO_2 Util. 18 (2017) 107–116.
614 [27] R. Zhang, N. Bassim, D.K. Panesar, Characterization of Mg components in reactive MgO
615 - Portland cement blends during hydration and carbonation, J. CO_2 Util. 27 (2018) 518–527.
616 [28] W. Shen, L. Cao, Q. Li, Z. Wen, J. Wang, Y. Liu, R. Dong, Y. Tan, R. Chen, Is magnesia
617 cement low carbon? Life cycle carbon footprint comparing with Portland cement, J. Clean.
618 Prod. 131 (2016) 20–27.
619 [29] L. Wang, L. Chen, D.C.W. Tsang, J.S. Li, T.L.Y. Yeung, S. Ding, C.S. Poon, Green
620 remediation of contaminated sediment by stabilization/solidification with industrial by-
621 products and CO_2 utilization, Sci. Total Environ. 631–632 (2018) 1321–1327.
622 [30] I. Taniguchi, T. Yamada, Low energy CO_2 capture by electrodialysis, in: Energy Proced.
623 (2017) 1615–1620.
624 [31] D. Xuan, B. Zhan, C.S. Poon, A maturity approach to estimate compressive strength
625 development of CO_2-cured concrete blocks, Cem. Concr. Compos. 85 (2018) 153–160.
626 [32] BS EN 12390, Testing Hardened Concrete Compressive Strength of Test Specimens.
627 British Standards Institution, London, UK (2009).

628 [33] L. Han, X. Li, J. Bai, F. Xue, Y. Zheng, C. Chu, Effects of flow velocity and different
629 corrosion media on the in vitro bio-corrosion behaviours of AZ31 magnesium alloy, Mater.
630 Chem. Phys. 217 (2018) 300–307.
631 [34] L. Wang, S.S. Chen, D.C.W. Tsang, C.S. Poon, K. Shih, Recycling contaminated wood
632 into eco-friendly particleboard using green cement and carbon dioxide curing, J. Clean. Prod.
633 137 (2016) 861–870.
634 [35] C. Unluer, A. Al-Tabbaa, Enhancing the carbonation of MgO cement porous blocks
635 through improved curing conditions, Cem. Concr. Res. 59 (2014) 55–65.
636 [36] L. Wang, L. Chen, D.W. Cho, D.C.W. Tsang, J. Yang, D. Hou, K. Baek, H.W. Kua, C.S.
637 Poon, Novel synergy of Si-rich minerals and reactive MgO for stabilisation/solidification of
638 contaminated sediment, J. Hazard. Mater. (2019) 695–706.
639 [37] D.K. Panesar, L. Mo, Properties of binary and ternary reactive MgO mortar blends
640 subjected to CO_2 curing, Cem. Concr. Compos. 38 (2013) 40–49.
641 [38] H. Chen, C. Zhao, Q. Ren, Feasibility of CO_2/SO_2 uptake enhancement of calcined
642 limestone modified with rice husk ash during pressurized carbonation, J. Environ. Manage. 93
643 (2012) 235-244.
644 [39] A. Coppola, A. Esposito, F. Montagnaro, G. De Tommaso, F. Scala, P. Salatino, Effect of
645 exposure to SO_2 and H_2O during the carbonation stage of fluidised bed calcium looping on the
646 performance of sorbents of different nature, Chem. Eng. J. (2018).
647
648

649 **Supplementary Information**

650 **Calculation of H_2SO_4 and HNO_3 dosage in MC and BC pastes**

651 Based on our field investigation, the typical CO_2, SO_2, and NO_2 concentrations in thermal
652 power plant exhaust are 7-12%, 3500-4500 mg Nm^{-3}, and 400-600 mg Nm^{-3}, respectively. In
653 this study, we assumed that **CO_2,** SO_2, and NO_2 concentrations from the thermal power plant
654 are **10%**, 4000 mg Nm^{-3}, and 500 mg Nm^{-3}, respectively; these **SO_2 and NO_2** concentrations
655 are equivalent to **0.14% and 0.024%** in the exhaust**,** respectively.

656

657 According to TGA results, the **CO_2 absorption extent is 4%** in the MC paste (CO_2
658 concentration of 100%, humidity of 98%). The reaction between acid gas and alkaline paste is
659 a diffusion-controlled reaction. Here, we assume that diffusion rates of acid gas are the same
660 as the rate of diffusion of CO_2 gas. Thus, the absorption extent of acid gas depends on the
661 concentration of acid gas in the exhaust.

662 We can calculate the dosage of H_2SO_4 and HNO_3 as follows:

663 $$m_{H2SO4} = 4\% \frac{0.14}{10} \times \frac{98}{44} \times 100\% = 0.125\%\ g$$

664 $$m_{HNO3} = 4\% \frac{0.024}{10} \times \frac{63}{44} \times 100\% = 0.0137\%\ g$$

665 Therefore, **H_2SO_4 (0.125 wt% of paste)** and **HNO_3 (0.0137 wt% of paste)** are added in the
666 specified mixtures, respectively.

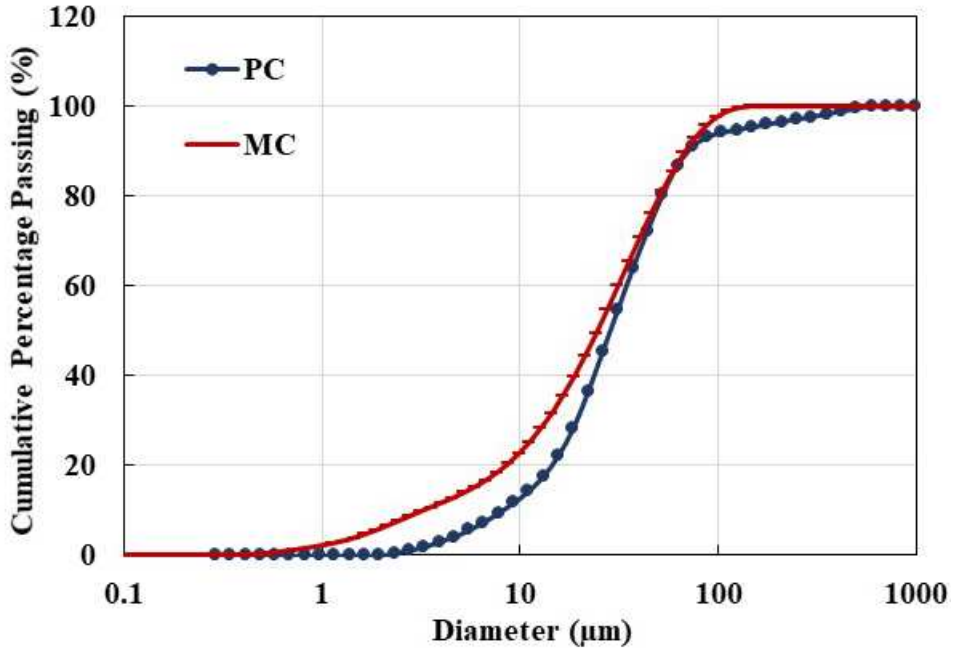

Figure S1. Particle size distribution of raw PC and MC.

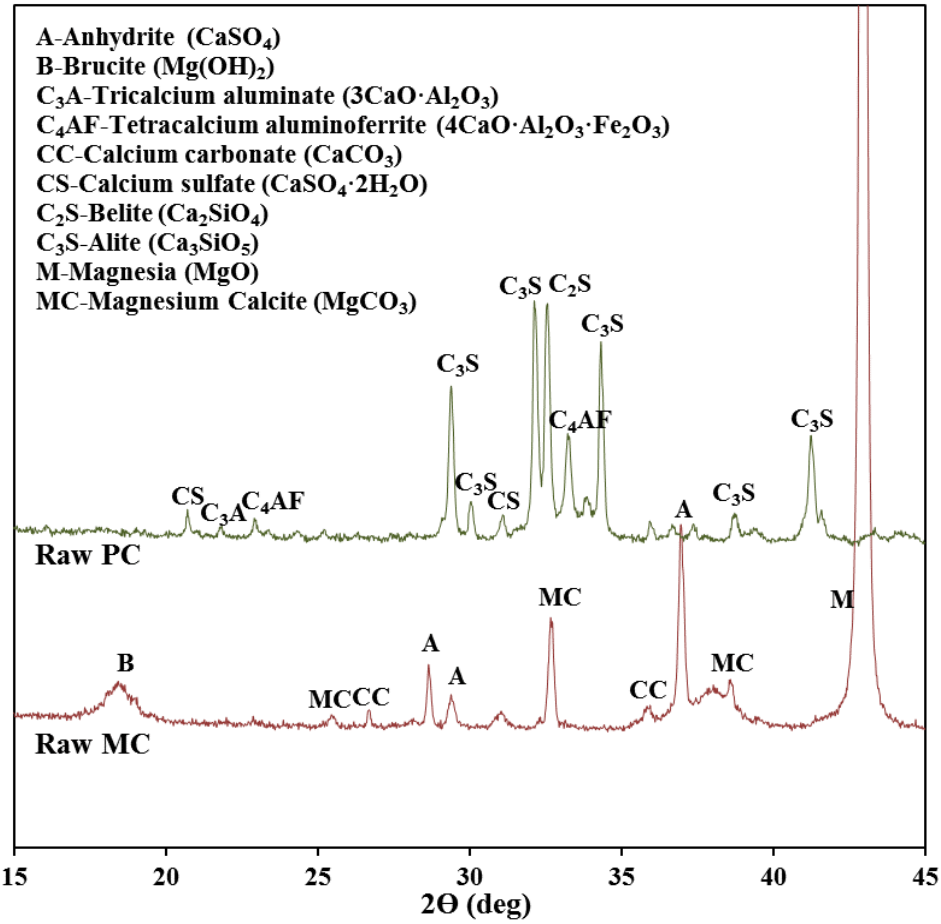

Figure S2. XRD diffractograms of raw PC and MC.

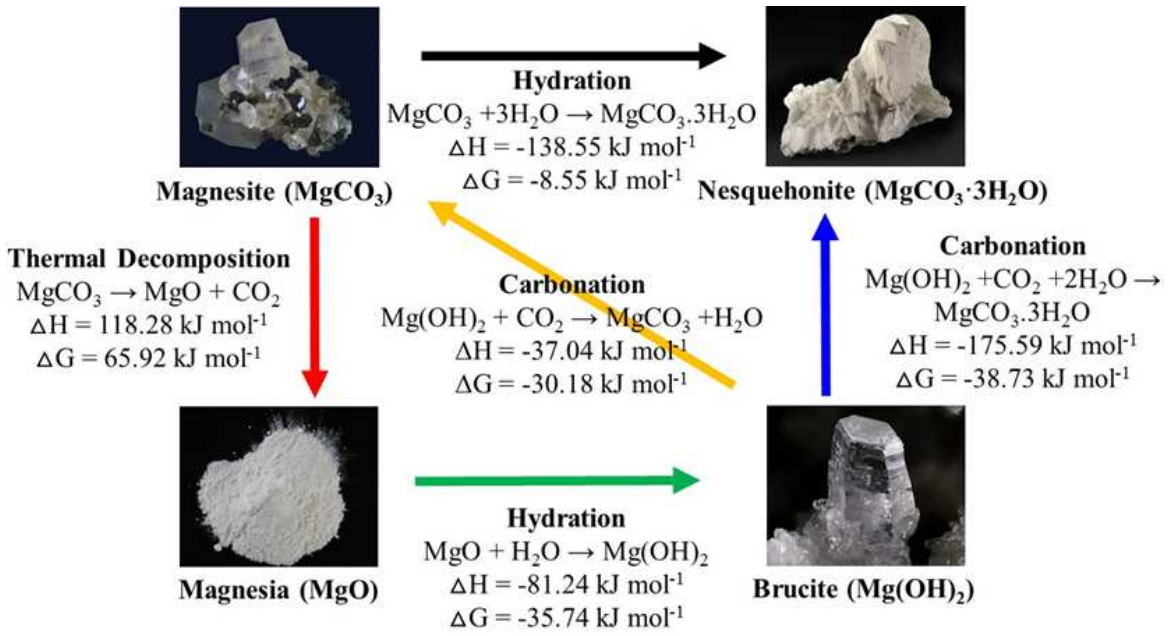

Figure S3. Thermodynamic reactions of the family of magnesium oxides/carbonates (Wang et al., 2016). Copyright Elsevier.

Reference:

Wang, L., Chen, S.S., Tsang, D.C.W., Poon, C.S., Shih K.M., 2016. Recycling contaminated wood into eco-friendly particleboard using green cement and carbon dioxide curing. J. Clean. Prod. 137, 861-870.

ELSEVIER LICENSE
TERMS AND CONDITIONS

Sep 19, 2019

This Agreement between Mr. liang chen ("You") and Elsevier ("Elsevier") consists of your license details and the terms and conditions provided by Elsevier and Copyright Clearance Center.

License Number	4672520469961
License date	Sep 19, 2019
Licensed Content Publisher	Elsevier
Licensed Content Publication	Journal of Cleaner Production
Licensed Content Title	Recycling contaminated wood into eco-friendly particleboard using green cement and carbon dioxide curing
Licensed Content Author	Lei Wang,Season S. Chen,Daniel C.W. Tsang,Chi-Sun Poon,Kaimin Shih
Licensed Content Date	Nov 20, 2016
Licensed Content Volume	137
Licensed Content Issue	n/a
Licensed Content Pages	10
Start Page	861
End Page	870
Type of Use	reuse in a journal/magazine
Requestor type	academic/educational institute
Intended publisher of new work	Elsevier
Portion	figures/tables/illustrations
Number of figures/tables/illustrations	1
Format	both print and electronic
Are you the author of this Elsevier article?	Yes
Will you be translating?	No
Original figure numbers	figures 1
Title of the article	Accelerated Carbonation of Reactive MgO and Portland Cement Blends Under Flowing CO2 Gas
Publication new article is in	Cement and Concrete Composites
Publisher of the new article	Elsevier
Author of new article	Lei Wang, Liang Chen, John L. Provis, Daniel C.W. Tsang, Chi-Sun Poon
Expected publication date	Jul 2019
Estimated size of new article (number of pages)	21
Requestor Location	Mr. liang chen ZS922, 9/F, Block Z, polyu

681